USGS
science for a changing world

Prepared in cooperation with Northern Arizona University

Monitoring Fine-Sediment Volume in the Colorado River Ecosystem, Arizona—Construction and Analysis of Digital Elevation Models

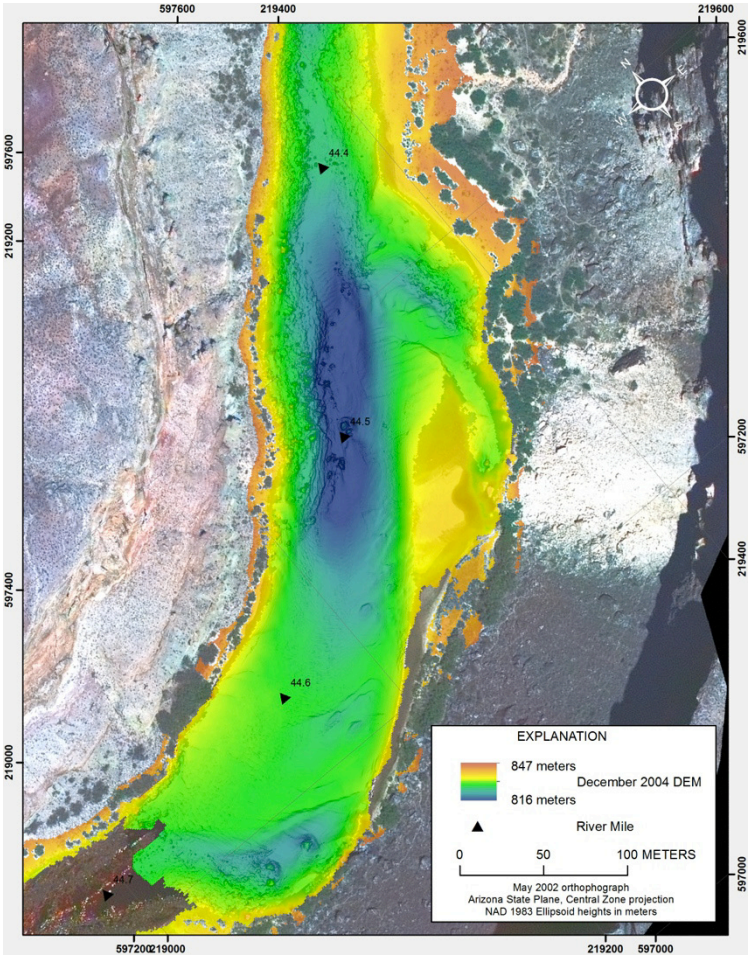

Open-File Report 2014–1052

U.S. Department of the Interior
U.S. Geological Survey

COVER
Digital elevation model (DEM) of a part of the Colorado River in Grand Canyon (river miles 44.3 to 44.7) in Grand Canyon National Park, Arizona. DEM is constructed from aerial lidar, ground topographic and multibeam bathymetry data collected in December 2004 and has a grid resolution of 1 meter.

Monitoring Fine-Sediment Volume in the Colorado River Ecosystem, Arizona—Construction and Analysis of Digital Elevation Models

By Matt Kaplinski, Joseph E. Hazel, Jr., Paul E. Grams, and Philip A. Davis

Prepared in cooperation with Northern Arizona University

Open-File Report 2014–1052

U.S. Department of the Interior
U.S. Geological Survey

U.S. Department of the Interior
KEN SALAZAR, Secretary

U.S. Geological Survey
Marcia K. McNutt, Director

U.S. Geological Survey, Reston, Virginia 2014

For product and ordering information:
World Wide Web: http://www.usgs.gov/pubprod
Telephone: 1-888-ASK-USGS

For more information on the USGS—the Federal source for science about the Earth,
its natural and living resources, natural hazards, and the environment:
World Wide Web: http://www.usgs.gov
Telephone: 1-888-ASK-USGS

Suggested citation:
Kaplinski, M., Hazel, J.E., Jr., Grams, P.E., Davis, P.A., 2014, Monitoring fine-sediment volume in the Colorado River ecosystem, Arizona—Construction and analysis of digital elevation models: U.S. Geological Survey Open-File Report 2014–1052, 29 p., *http://dx.doi.org/10.3133/ofr20141052.*

ISSN 2331-1258 (online)

Contents

Figures

Tables

Appendix

[Available online only at http://pubs.usgs.gov/of/2014/1052/]

Conversion Factors

Inch/Pound to SI

Multiply	By	To obtain
	Length	
foot (ft)	0.3048	meter (m)
mile (mi)	1.609	kilometer (km)
	Area	
square foot (ft^2)	0.09290	square meter (m^2)
	Volume	
cubic foot (ft^3)	0.02832	cubic meter (m^3)
	Flow rate	
cubic foot per second (ft^3/s)	0.02832	cubic meter per second (m^3/s)

SI to Inch/Pound

Multiply	By	To obtain
	Length	
meter (m)	3.281	foot (ft)
kilometer (km)	0.6214	mile (mi)
	Area	
square meter (m^2)	10.76	square foot (ft^2)
	Volume	
cubic meter (m^3)	35.31	cubic foot (ft^3)
	Flow rate	
cubic meter per second (m^3/s)	35.31	cubic foot per second (ft^3/s)

Temperature in degrees Celsius (°C) may be converted to degrees Fahrenheit (°F) as follows:
°F=(1.8×°C)+32
Temperature in degrees Fahrenheit (°F) may be converted to degrees Celsius (°C) as follows:
°C=(°F-32)/1.8
Vertical coordinate information is referenced to the insert datum name (and abbreviation) here, for instance, "North American Vertical Datum of 1988 (NAVD 88)"
Horizontal coordinate information is referenced to the insert datum name (and abbreviation) here, for instance, "North American Datum of 1983 (NAD 83)"
Altitude, as used in this report, refers to distance above the vertical datum.

Monitoring Fine-Sediment Volume in the Colorado River Ecosystem, Arizona—Construction and Analysis of Digital Elevation Models

By Matt Kaplinski,[1] Joseph E. Hazel, Jr.,[1] Paul E. Grams,[2] and Philip A. Davis[2]

Abstract

Digital elevation models (DEMs) of eleven 2–5 kilometer reaches of the Colorado River ecosystem (CRE) in Grand Canyon were constructed from repeat bathymetric and topographic surveys collected between August 2000 and December 2004. The DEMs will be used by researchers to study the effects of Glen Canyon Dam (GCD) operations on the sediment resources of the CRE in Grand Canyon by quantifying morphological changes and sediment transfer within and among the study reaches.

Airborne surveys collected light detection and ranging (lidar) and photogrammetric data, whereas ground topographic and bathymetric data were collected simultaneously on river trips. Surveys were conducted in August 2000, September 2000, May 2002, May 2004, November 2004, and December 2004. The aerial lidar and photogrammetric data were merged with the ground topographic and bathymetric data to create DEMs of the study areas with a grid resolution of 1 meter. For each survey period, the vertical component of uncertainty (specifically, reproducibility or precision) was estimated for each data type (lidar/photogrammetry, ground surveys, bathymetry) and for two different types of bed-surface texture (smooth and rough).

The resulting DEMs from this study are a valuable contribution to ongoing efforts in assessing the effects of GCD operations on the CRE. The DEMs can be used to map the spatial characteristics of geomorphic change within the study reaches and to estimate sediment budgets for different time periods by calculating the difference in sediment volume between surveys. In addition, the DEMs provide essential boundary conditions for numerical models of sediment transport and deposition, as well as help define the spatial distribution of habitat for fisheries investigations.

Introduction

The existence and operation of Glen Canyon Dam (GCD) has altered the morphology and ecology of the Colorado River in Grand Canyon (Webb and others, 1999; Gloss and others, 2005). For example, both the distribution and volume of fine-grained sediment deposits have been extensively altered as a result of changes in the flow regime and the upstream impoundment of sediment. Pre-dam seasonal variability in the river's flow rate, which included spring snowmelt floods, has been replaced with a diurnally fluctuating flow regime that varies in response to demands for hydroelectric power. In the post-dam era, the Paria and Little Colorado Rivers are the primary sources of fine-grained sediment to the river downstream of GCD. These tributaries supply only 15 to 20 percent of the pre-dam sediment load (Topping and others, 2000). Studies have shown that the number and size of sandbars have substantially decreased in response to the change in flow and decrease in sediment supply (Schmidt and

[1]Northern Arizona University, School of Earth Sciences and Environmental Sustainability.
[2]U.S. Geological Survey, Grand Canyon Monitoring and Research Center.

Graf, 1990; Webb and others, 1999; Wright and others, 2005). Sandbars along the Colorado River in Grand Canyon are an important component of the ecosystem because they provide camp sites for river runners and hikers, crucial substrates for riparian vegetation that serve as wildlife habitats, protect pre-dam deposits that contain culturally important archeological sites, and are an integral component of the natural landscape (Webb and others, 1999). An important goal of ongoing geomorphic research in Grand Canyon is to monitor sandbars and the status of fine-grained sediment storage to inform resource managers about the effectiveness of management efforts to maintain a positive sediment balance in the system and thereby rebuild degraded sandbars (U.S. Department of the Interior, 1995).

The U.S. Geological Survey (USGS) Grand Canyon Monitoring and Research Center (GCMRC) has developed a comprehensive monitoring and research program to study the effects of GCD operations on the sediment resources of the Colorado River ecosystem (CRE) in Grand Canyon. This program is based on a sediment budget paradigm and consists of three integrated components:

Monitoring suspended sediment transport (Topping and others, 2010).

Measuring topographic change in sediment deposits by repeat total-station and bathymetric surveys (Hazel and others, 2010).

Modeling sediment transport and sandbar morphodynamics (Wright and others, 2010; Logan and others, 2010).

This report presents methods and data collected in support of the topographic change component of this monitoring program.

Technological advances made over the past decade have made it possible to rapidly acquire highly accurate topographic and bathymetric data over large areas. Geomorphologists now routinely use these technologies to investigate fluvial processes and monitor geomorphic change (Brasington and others, 2003; Lane and others, 2003; Wheaton and others, 2010). Digital elevation models (DEMs) derived from such periodic surveys accurately record landform surface variations, which are used to quantify and monitor morphological changes and sediment transfer across a variety of spatial scales. In this study, repeat topographic and bathymetric surveys of 11 reaches, ranging in length from 2–6.5 kilometer (km), of the Colorado River in Grand Canyon were conducted. The hybrid topographic surveys combined light detection and ranging (lidar) and photogrammetric topographic data from airborne surveys with ground-based and boat-based topographic and bathymetric data collected during waterborne survey trips. All of these surveys were combined to construct DEMs of the river reaches. This report outlines the procedures used to collect and process the hybrid topographic data, to construct the DEMs, and to estimate the spatially distributed uncertainty associated with the DEMs.

Study Area, Place Names, and Units

The study area is the Colorado River corridor within Glen, Marble, and Grand Canyons in northern Arizona (fig. 1). Locations discussed in this report are referenced by the GCMRC river mile (RM) system, which is distance in miles along the channel centerline downstream from Lees Ferry, Arizona (U.S. Geological Survey, 2006). Lees Ferry (RM 0) is located 15.5 miles downstream from GCD and 1 mile upstream from the mouth of the Paria River and the northeastern boundary of Grand Canyon National Park (fig. 1). Glen Canyon extends from GCD to Lees Ferry. Marble Canyon begins at the mouth of the Paria River and extends downstream to the Little Colorado River confluence. Although Marble Canyon is within Grand Canyon National Park, this report refers to Grand Canyon as the reach of the Colorado River that extends from the Little Colorado River confluence downstream to Diamond Creek (RM 226).

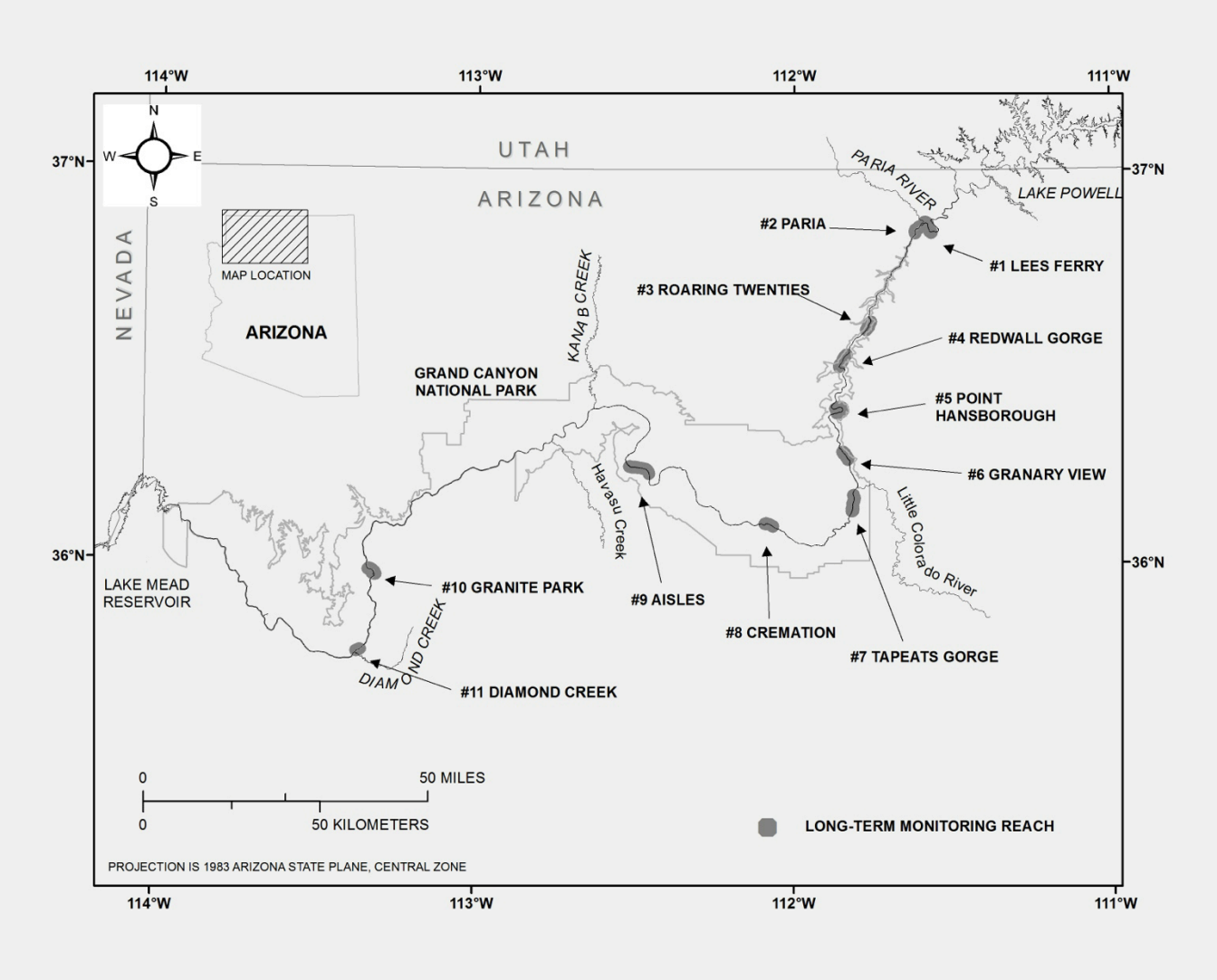

Figure 1. Map showing location of study reaches along the Colorado River corridor within Glen, Marble, and Grand Canyons, Arizona.

To integrate topographic datasets from different sources into a composite DEM, all topographic and bathymetric data were processed in the State Plane Coordinate System, Central Arizona, zone map projection in meters using the NAD83 (2011) vertical datum. Elevations are reported as ellipsoid heights (EH) because the national geoid model does not incorporate sufficient gravity measurements in the Grand Canyon region to account for the large variation in crustal mass along the river corridor (Saleh and others, 2003).

In this report, we define the term DEM as a "bare earth" elevation model that represents the ground surface that is free of vegetation, the surfaces of standing bodies of water, and other "nonground" objects (for example, power cables, buildings, and other structures), whereas, a digital surface model (DSM) refers to an elevation model that includes the tops of vegetation, standing bodies of water, and any other objects.

Study Reaches

Eleven river reaches were selected for study within the CRE in Glen, Marble, and Grand Canyons, Arizona (fig. 1). The reaches are numbered increasing downstream from GCD (table 1). Some

of the reaches were surveyed multiple times, whereas some reaches were surveyed less frequently (table 2). Four reaches (reaches 2, 4, 5, and 7) were initially surveyed in August and September 2000 (Schmidt and others, 2007). In 2002, all 11 reaches were surveyed, whereas only reaches 2 through 8 were surveyed in May 2004, and reaches 2 through 7 were surveyed in November and December 2004. This report focuses on reaches 2 through 7, as these are the only reaches that include repeat surveys. Reaches 2 through 7 have a total length of 22.2 km, which is 21 percent of the total channel length between RM 0 and RM 66.4. The individual reaches range in length from 1.3 to 6.4 km and have an average length of 3.5 km. Reaches 2 through 6 are located in Marble Canyon; reach 7 is in Grand Canyon, 3 km downstream from the Little Colorado River confluence.

Table 1. Characteristics of the study reaches along the Colorado River corridor within Glen, Marble, and Grand Canyons, Arizona.

Long-term monitoring reach		River mile[1]		Average channel width[2], in meters	Channel slope[3]
Number	Local name	Starting	Ending		
1	Lees Ferry	-2.4	0	123	0.0001
2	Paria	1.1	2.7	113	0.0002
3	Roaring Twenties	21.9	23.7	56	0.0016
4	Redwall Gorge	29.4	32.1	64	0.0009
5	Point Hansborough	42.5	45.5	82	0.0009
6	Granaries	54.5	56.3	90	0.0003
7	Tapeats Gorge	63.4	66.4	95	0.0012
8	Cremation	86.6	88.1	64	0.0020
9	Aisles	119.3	123.3	65	0.0010
10	Granite Park	207.7	209.2	72	0.0013
11	Diamond Creek	224.8	225.6	66	0.0002

[1]Based on the river mile centerline (U.S. Geological Survey, 2006) downstream from Lees Ferry (river mile 0), in Grand Canyon National Park except, the Lees Ferry reach, which is in Glen Canyon National Recreation Area.

[2]At 227 cubic meters per second (m^3/s), average based on cross section data from Magirl and others (2005).

[3]Based on measured water-surface elevations at a steady discharge of 227 m^3/s.

Table 2. Data types collected in study reaches along the Colorado River corridor within Glen, Marble, and Grand Canyons, Arizona, during each monitoring period.

Long-term monitoring reach		Monitoring year and data types[1] collected					
Number	Local name	Aug. 2000	Sept. 2000	May 2002	May 2004	Nov. 2004	Dec. 2004
1	Lees Ferry			A, C, D, E			
2	Paria	A, B, D	A, B, D	A, C, D, E	A, D	A, B, D	A, B, D
3	Roaring Twenties			A, C, D, E	A, D	A, B, D	A, B, D
4	Redwall Gorge	A, B, D	A, B, D	A, C, D, E	A, D	A, B, D	A, B, D
5	Point Hansborough	A, B, D	A, B, D	A, C, D, E	A, D	A, B, D	A, B, D
6	Granaries			A, C, D, E	A, D	A, B, D	A, B, D
7	Tapeats Gorge	A, B, D	A, B, D	A, C, D, E	A, D	A, B, D	A, B, D
8	Cremation			A, C, D, E	A, D		
9	Aisles			A, C, D, E			
10	Granite Park			A, C, D, E			
11	Diamond Creek			A, C, D, E			

[1]Data types: A, total station surveys; B, lidar; C, photogrammetry; D, bathymetric surveys; E, multispectral digital imagery.

Data Collection and Processing

In Marble and Grand Canyons, sediment storage is concentrated in eddies and the adjacent channel (Hazel and others, 2006; Grams and others, 2013). One of the objectives of this mapping effort is to determine the distribution of these storage locations, which requires mapping as much of each study reach as possible. To accomplish this goal, a combination of remotely sensed and ground-based data were collected in August 2000, September 2000, May–June 2002, May–June 2004, November 2004, and December 2004 (fig. 2, table 3). Channel bathymetry was mapped by multibeam and singlebeam sonar and subaerial topography was mapped by airborne lidar, aerial photogrammetry, and ground-based total-station (table 2). Lidar and photogrammetric data were collected during aerial overflights that typically spanned a 4–6 day period. Ground-based topographic and bathymetric data were collected on research river trips lasting 14 to 20 days. To prevent error due to topographic change over the data collection period, the airborne and ground data collections were coordinated to minimize the time difference between collection of the datasets for a given time period.

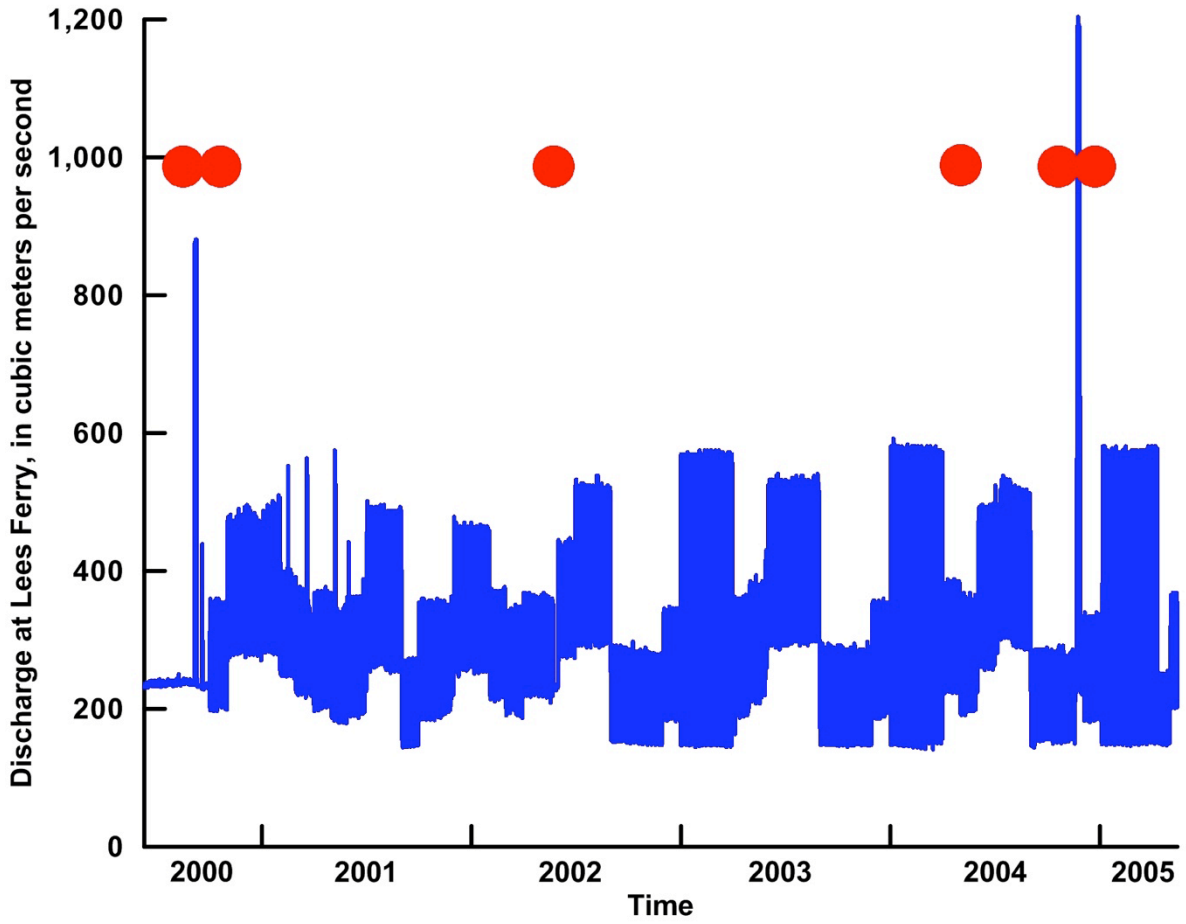

Figure 2. Discharge hydrograph from U.S. Geological Survey gaging station Colorado River near Lees Ferry (Blue, station 09380000), Arizona, during the period of study. Dates of airborne and ground-based survey trips are show by red dots. Note the daily and seasonal fluctuations in flow volume, the Low Steady Summer Flow (LSSF) experiment in 2000 that included a powerplant capacity-flow (~878 cubic meters per second, m^3/s) event, and the High-Flow Experiment event (1,161 m^3/s) in November 2004.

Table 3. Dates of data collection in the Colorado River corridor within Glen, Marble, and Grand Canyons, Arizona.
[Date format is Month/Day; n.a., not applicable]

Data collection method	August 2000	September 2000	May 2002	May 2004	November 2004	December 2004
Lidar	8/29–8/31	9/15–9/18	n.a.	n.a.	11/19–11/21	12/07–12/09
Photogrammetry	n.a.	n.a.	5/24–6/05	n.a.	n.a.	n.a.
Total station	8/19–8/27	9/03–9/17	4/28–5/16	5/29–6/9	11/12–11/20	12/1–12/10
Multibeam bathymetry	8/19–8/27	9/03–9/17	4/28–5/16	5/29–6/9	11/12–11/20	12/1–12/10
Singlebeam bathymetry	8/19–8/27	9/03–9/17	n.a.	n.a.	n.a.	n.a.

The following sections briefly summarize the individual components of the ground-based data collections, including the control network, total-station method, and bathymetric method, because they have been previously described in detail (Hazel and others, 2008; Kaplinski and others, 2009). The airborne data collections and processing methods are discussed in greater detail because they have not been previously described elsewhere.

Geodetic Control Network

All airborne and ground-based surveys are referenced to a geodetic control network developed by the GCMRC (Hazel and others, 2008). The control network consists of 16 primary control benchmarks that were established along the canyon rim and connected to the National Spatial Reference System (Doyle, 1994), with secondary and tertiary points located along the river corridor. Secondary control points along the river corridor were established by simultaneous Global Positioning System (GPS) occupations with the established rim-control points using the procedures described by Zilkoski and others (1997). Tertiary control points were referenced to the secondary point network using conventional survey techniques. The secondary and tertiary control points are stable survey marks monumented with a chiseled or scribed X, P-K masonry nail, or carriage bolt. The accuracy of the primary rim control network is constrained to 0.02 meters (m) vertical and 0.02 m horizontal, whereas secondary and tertiary points have a positional error less than 0.03 m and a vertical error between 0.01 and 0.10 m, at 95-percent confidence level (Hazel and others, 2008).

Ground-Based Topographic Surveys

Ground-based collection of topographic data was undertaken using total-station survey methods. The narrow canyon setting and associated environmental conditions preclude the use of kinematic-GPS techniques for rapid acquisition of field-survey data (Hazel and others, 2008). As a result, conventional total-station surveying provided the means for collecting high-accuracy topographic data and for accurate positional referencing of the bathymetric data. The following data were collected or established using conventional total-station (TS) surveying techniques and are hereafter referred to as TS points: (1) topographic data, (2) check points for ground-truthing lidar data, (3) temporary benchmarks for bathymetric navigation shore stations or for additional total-station locations, and (4) locations of subaerial and subaqueous sample sites (for example, scour chains, digital microscopes, and video cameras). Benchmark and backsite coordinates were verified at all total station positions by comparing field measurements with benchmark coordinates in the GCMRC control network. Vertical and horizontal accuracies of the surveyed checkpoints (at the 95-percent confidence level) within the study areas were less than or equal to 0.05 m (Hazel and others, 2008). The TS points were edited, processed and checked for errors (such as rod height and coding mistakes), then exported to ASCII files containing the coordinate values in meters (northing, easting, EH) and surface-descriptor code for each point.

Bathymetric Surveys

Bathymetric data covered the largest part of the study reaches and comprise approximately 74 percent of the total DEM area. The bathymetric data collection system used a robotic total station, or shore station, to provide line-of-sight navigation data (Kaplinski and others, 2009). Shore stations are established on benchmarks referenced to the geodetic control network, and the data collected from each shore station location is treated as an individual survey. Each study reach required from 4 to 8 individual surveys to complete the mapping. The August and September 2000 data collections included both singlebeam and multibeam sonar, whereas subsequent data collections only used multibeam sonar (Kaplinski and others, 2009). Three individual surveys were collected using the singlebeam system in August 2000, whereas five individual surveys were collected in September 2000. Singlebeam data were collected by following a 10-m grid pattern along planned lines. The singlebeam soundings were manually edited to remove erroneous soundings and then filtered to output one point per meter along the vessel trackline, which results in a point density of approximately 0.2 points/square meter (points/m^2). Soundings were filtered to optimize the generation of the triangulated irregular network (TIN) surface model of the topographic surface. All other parts of the study reaches were mapped using the multibeam system. This system collects approximately 1 to 5 million soundings per survey. Multibeam soundings were filtered by calculating the median elevation of soundings within 0.25-m and 1.0-m grid cells. The data filtered to 1-m resolution were used to construct the bathymetry part of the DEMs, and the data filtered to 0.25 m were used for bed-texture analysis. The 1-m grid resolution was selected by using a grid-size estimator (see section on DEM Construction) to determine the appropriate cell size for the hybrid datasets. This resolution is both computationally efficient and resolves the scale of features necessary for volume calculations. The number of soundings per square-meter grid cell varies from 1 to 3,000, with an average of approximately 200 soundings per cell. All bathymetric data were collected and processed using Hypack and Hysweep software, and the filtered data were exported as ASCII files containing the coordinates and EH for each point.

Airborne Lidar and Photogrammetric Surveys

Data Collection

The above-water topography was mapped with airborne lidar and stereo panchromatic imagery, supplemented with ground-based total station surveys (Davis, 2004). Topographic data were extracted photogrammetrically from imagery collected in 2002. All other overflights collected lidar data using a variety of sensors (table 4). Unfortunately, the lidar collection system malfunctioned during the May 2004 mission, and the data are, therefore, excluded from this study. All of the successful aerial-survey data were collected using fixed-wing aircraft flying at 100-knots at altitudes above 1,250 m; different laser pulse rates of the various lidar sensors produced a range of point densities (0.37 to 5.18 points/m^2) in the final lidar point datasets (table 4).

Table 4. Lidar and photogrammetry sensor characteristics used in this study along the Colorado River corridor within Glen, Marble, and Grand Canyons, Arizona.

[mm, millimeters; cm, centimeters; m, meters; m^2, square meters; km, kilometers; kHz, kilohertz; mrad, milliradians; AGL, above ground level; k, thousand; n.a., not applicable; GPS, Global Positioning System; CCD, charge-coupled device]

Characteristics	RAMS[1] lidar	RAMS lidar	ISTAR[2] (HRSC-AX[4])	DATIS III[3] lidar	RAMS lidar
Collection dates	Aug., 2000	Sept., 2000	May, 2002	Nov., 2004	Dec., 2004
Flight AGL (m)	1,250	1,250	6,096	1,828	1,250
Base stations per study area	1	1	1	2	2
Average baseline distance (km)	30	30	20	20	20
GPS recording interval (seconds)	1	1	1	1	1
Minimum GPS satellites used	5	5	6	6	6
Pulse rate (kHz)	15	15	n.a.	36.5	35
Scan rate (Hz)	13.4	13.4	n.a.	28	24.2
Swath width (m)	230	230	2,640	840	305
Beam divergence (mrad)	0.33	0.33	n.a.	0.25	0.33
Scan half angle (degrees)	5	5	15	13	7
Laser footprint (m)	0.4	0.4	n.a.	0.46	0.4
Along-track spacing (m)	1.4	1.5	0.22	2.2	2.3
Across-track spacing (m)	1.7	1.6	0.22	1	0.7
Line point density (points/m^2)	0.37	0.44	21	0.5	0.57
Flight-line replications	21	21	6	4	4
Final point density (points/m^2)	0.37	0.44	1	3.52	5.18
Returns	2	2	n.a.	2	2
Intensity recorded	No	No	n.a.	Yes	Yes
Average noise level (cm)[5]	7.5	7.8	3.7	9.7	7.7
Recording media (CCD elements)	4k×4k	4k×4k	12k×12k	None	None
Focal length (mm)	90	90	151	n.a.	n.a.
Image resolution (cm)	18	18	22	n.a.	n.a.
Image bit-type	8	8	8	n.a.	n.a.

[1]RAMS, Remote Airborne Mapping System, Enerquest, Colorado.

[2]ISTAR, Imagerie Stereo Appliquee au Relief, France.

[3]DATIS III, Digital Airborne Topographic Imaging System, 3-Di Technology, Maryland.

[4]HRSC-AX, High Resolution Stereo Camera, aerial, version X.

[5]Determined using method of Crombaghs and others (2002).

Strict requirements were placed on all of the airborne data collections to optimize the accuracy and precision of their collected data. These specifications required that (1) at least five to six GPS satellites be within view (greater than15º above the horizon) and recorded during all airborne collections to provide position dilution of precision (PDOP) values less than 2.5, (2) at least two GPS base stations be operating within 30 km of any airborne collection and that all base-station data be used in the data processing, (3) lidar data collections use a maximum scan half-angle of 15º (to limit beam eccentricity), (4) the lidar ground spot diameter be less than 0.5 m (to reduce uncertainties as to the location and surface material that produced the measured laser return), and (5) lidar flightlines be collected four times and, because vertical offsets were observed among repetitive flight lines, each processed lidar flightline be delivered as a separate point file. The sensor characteristics and collection parameters for each of the airborne surveys are summarized in table 4.

During each airborne survey, primary control points along the canyon rim were occupied with GPS receivers. These receivers recorded the dual frequency (L1/L2) carrier phase and pseudo-range measurements from each GPS satellite in view. During the 2000 airborne surveys, only one base station per study area was occupied, but all subsequent collections had at least two base stations that operated within a 30-km radius of each study site. All aircraft used for the data collections were equipped with a

similar GPS unit, as well as an Inertia Measurement Unit (IMU) to record the aircraft motion and heading. The canyon-rim base stations and the aircraft GPS/IMU systems used a one-second recording epoch. Before data collection, the aircraft passed over operating base stations to assure that on-the-fly integers were correctly fixed during the postprocessing phase. During postprocessing, the base-station GPS data were processed in static mode to verify their published positions and to detect problems. The airborne GPS/IMU data were then processed with the base-station data in both forward and reverse chronologic directions to obtain trajectory positions. The lidar data were processed to determine the northing, easting, and EH coordinates of each laser return and to remove obvious anomalies in each flightline.

The May 2002 photogrammetric data were derived from digital panchromatic stereo imagery using softcopy photogrammetry. The imaging sensor was a high-resolution, push-broom camera system (the HRSC-AX). The sensor simultaneously collected three ground lines of data using three separate optics—one lens looked forward (+20.5º), one looked nadir, and the other lens looked backward (−20.5º) along the flight path. Multiple (five or six) overlapping flight lines provided a minimum of five stereo looks for each ground element. Each of the three panchromatic sensors had a 12,000-element charged-coupled device (CCD) that provided 0.22 m ground resolution at the flight altitude of 6,096 m using a 151-mm lens. Automatic triangulation was performed on the raw panchromatic image data using the on-board IMU and GPS data, the canyon-rim GPS base-station data, and the ground control panels that were placed throughout the study areas before airborne data collection. A DSM was produced from these data with a 1-m cell size.

Land-Cover Maps for Lidar Postprocessing

Preliminary examination of the lidar and photogrammetry datasets indicated that additional postprocessing was required to improve accuracy and consistency among the datasets. The issues that were observed in the lidar data included: (1) anomalous Ellipsoid Height (EH) values (data spikes) along the shoreline, (2) elevation differences (ΔEH) between flight-line and ground checkpoint EH values, and (3) vertical error increasing with slope, which suggested planimetric error. The two issues related to the photogrammetry data were vertical offset and horizontal tilt (from river right to river left) in delivered DSM surfaces. A series of processing procedures were applied to the lidar and for each study area and for each data collection period. The land-cover units were defined based on surface types that affect the accuracy of elevations determined by lidar. The land-cover units consisted of bare, smooth ground; bare, rough ground; standing water; damp ground; sparsely vegetated surfaces; and densely vegetated surfaces (fig. 3). These surfaces were initially identified and mapped using the color-infrared (CIR) photogrammetry data to resolve these issues. However, lidar mapping is more complex than photogrammetric mapping because the accuracy of lidar varies depending on land-cover characteristics (for example, smooth bare ground, rough bare ground, damp ground, vegetation cover) and local slope (for example, Bowen and Waltermire, 2002; Raber and others, 2002; Hodgson and others, 2003; Peng and Shih, 2006). To treat such surfaces separately in the lidar postprocessing stage, land-cover maps were produced from imagery that was collected in May 2002 and orthorectified to a 0.25-m positional accuracy. This imagery has a 0.44-m spatial resolution, which is 2.5 times higher resolution than the 1-m resolution of the final DEMs.

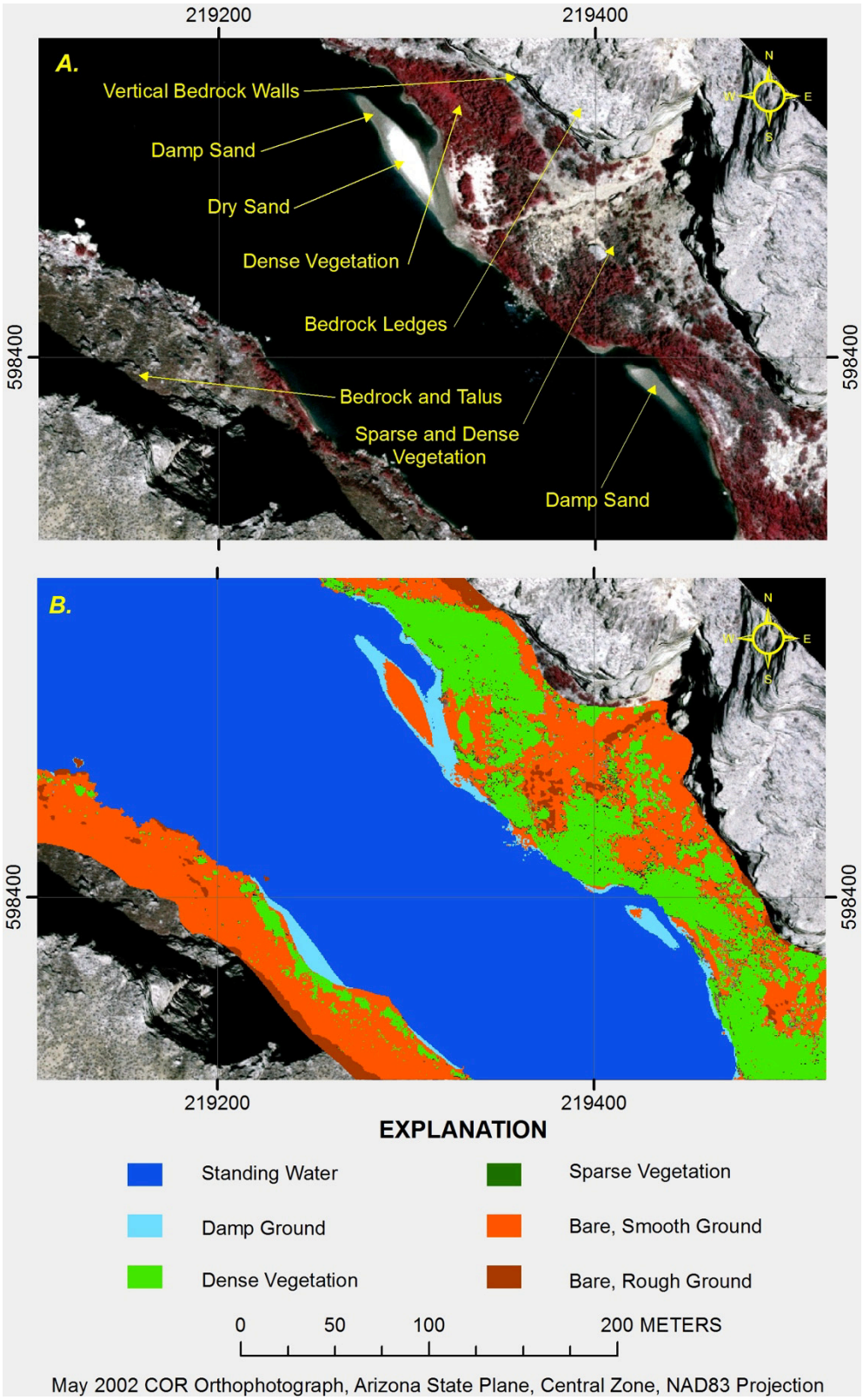

Figure 3. Map of a part of reach 5 showing the different landform surfaces in along the Colorado River corridor in Grand Canyon, Arizona. *A*, May 2002 color-infrared image showing examples of a variety of landform features. *B*, May 2002 land-cover classification map for same area shown in *A*.

All of the lidar sensors that were used in this study also collected either digital imagery or laser-return intensity. With sufficient spot density (4–5 points/m^2) laser-return intensity data (in raster-image form) look quite similar to digital panchromatic imagery at 0.50-m resolution and can be used to determine changes in surface cover between consecutive surveys. All of the raster-image and intensity-image data collected during our lidar surveys were registered to the May 2002 image base. The initial May 2002 land-cover map for each study site was then modified for the different lidar collection periods using the images from each collection period.

Three additional datasets were derived for each study site to facilitate error checking and quantification of uncertainty. Those datasets are (1) a local slope map, because vertical error increases with increasing slope; (2) a river-stage map that includes the 2,746 cubic meters per second (m^3/s) stage elevation, above which there has been essentially no change throughout the collection periods and provides fiducial areas for calibration; and (3) a map of the orthogonal distance from the river's centerline, which was used to examine potential topographic asymmetry. Each point within each lidar point file (consisting of northing, easting, EH, return, and intensity) was then classified according to corresponding land-cover unit, and local slope.

Postprocessing Airborne Topographic Data

The first procedure applied to the lidar data was the detection and removal of shoreline data spikes, which are randomly occurring, anomalously high lidar EH values within 1–2 m of the water's edge. The data spikes were most likely produced by sun glint, which produces an anomalous energy pulse to the lidar sensor when the lidar sensor is looking in the direction of the solar azimuthal angle and the Sun's incidence angle on the water surface equals the airborne laser receiver's look angle. To detect and remove these spikes, a modified Crombaghs and others (2002) method was used to determine local, inherent noise levels in each lidar dataset; shoreline point values that exceeded their surrounding point values by at least two levels of local noise were deemed anomalous and were removed from the point file.

Lidar scan lines can be vertically and planimetrically shifted from true ground positions due to (1) inherent error in the GPS and IMU systems, (2) misalignment of the integrated GPS-IMU system on the aircraft, or (3) error in processing the GPS-IMU data. Vertical offsets and planimetric errors were minimized in the datasets using a second procedure, which applied an iterative procedure that uses a data-driven approach (Filin, 2003), whereby point or DSM data are transformed (via translation, rotation, or polynomial corrections) so that the difference between a particular data collection and a reference surface is minimized (for example, Postolov and others, 1999; Crombaghs and others, 2000; Maas, 2000; Kager and Kraus, 2001; Maas, 2002).

The first step in the second procedure provided initial estimates of vertical error by comparing flight-line data to (1) ground-truth checkpoints or TS points, (2) other flight-line data acquired the same day (intracollection comparison), and (3) other flight-line data acquired in different years (intercollection comparison). The latter comparisons were restricted to areas not inundated in the intervening period (above the 1,275 m^3/s flow stage). All three types of comparisons used only bare, relatively flat (slope less than or equal to 11°) areas. A least squares (LSQ) analysis of the all pairs of flight-line ΔEH values was then applied to determine the initial vertical offsets for each lidar flight line. The points in each lidar flight line were adjusted using these initial estimates of vertical offset.

In the second step, each lidar flight line was examined to detect and correct planimetric error using the approach of Maas (2002), which compares each flight-line scan with a reference DSM. Planimetric corrections (northing and easting adjustments) were determined for every point within a flight line by performing a LSQ analysis iteratively on various northing and easting DSM cell shifts to derive the northing-easting shifts that most closely produced target-surface and reference-surface coincidence. The reference (or fiducial) surface for each study site was selected by producing shaded-

relief images of all lidar flight lines using the solar-elevation and solar-azimuthal angles that existed when the well-controlled, CIR imagery was acquired in May 2002. The shaded-relief, flight-line image that by visual inspection most closely matched the orthorectified CIR imagery above the 1,275 m^3/s flow stage was selected as the fiducial surface for that study area. In most cases, the December 2004 flight lines were selected as the fiducial surface. Fortunately, both sides of the river corridor have numerous, abrupt bedrock scarps that made planimetric shift determinations easy and accurate. After all scanline points within each lidar flight line were analyzed the resulting point shift values were applied to the original lidar point datasets. In the final step, the true vertical offset for each planimetrically adjusted lidar flight line was determined and applied to produce corrected EH values for each flight line. The flight-line vertical offsets ranged from −0.18 to 0.45 m, but the majority were less than +/-0.01 m.

The 2002 photogrammetric DSM had a vertical offset of 0.35 m within all study sites; the DSM EH values were adjusted downward by this offset. Comparison of the photogrammetric DSM with each study site's reference DEM indicated that the photogrammetric DSM also had cross-channel tilt, which varied within the longer reaches. The magnitude and direction of surface tilt within each study site was determined by comparing centerline transects of the reference DSM and photogrammetric DSM every meter (or DSM cell) along the river's centerline, above the 1,275 m^3/s flow stage. The photogrammetric DSMs were then adjusted using the ΔEH between the transects. The corrected DSMs were exported in ASCII format, so that the data could be further processed in the same manner as the other point datasets.

DEM Construction

A link to digital products for this study that are posted on the USGS Grand Canyon Monitoring and Research Center (GCMRC) Web site, including DEMs and associated uncertainty surfaces, is available at http://pubs.usgs.gov/of/2014/1052/.

The combined hybrid data point files (northing, easting, EH) were used to construct DEMs of the channel bed and banks for each reach and each monitoring period (fig. 4; table 5; appendix 1, available online only at http://pubs.usgs.gov/of/2014/1052/). The DEMs were constructed in ESRI's ArcGIS 3D analyst extension. The general approach was to create a TIN model from the hybrid datasets, then interpolate a 1-m raster DEM from the TIN model using a natural neighbors interpolation method. Creating the TIN models, therefore, is a crucial stage in the process and required several processing steps to ensure the model best represented the ground surface at the time of the surveys.

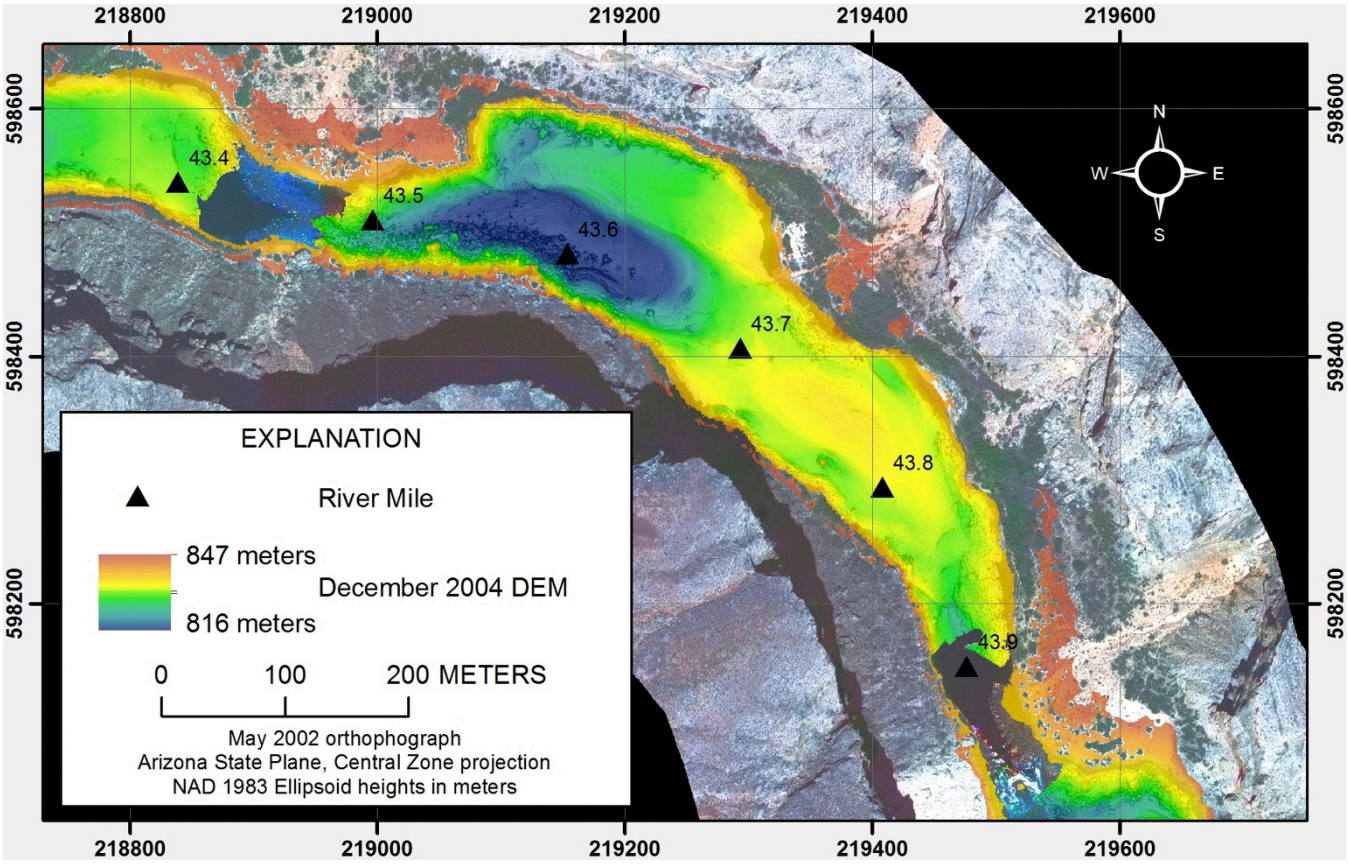

Figure 4. Map of a part of reach 5 in Grand Canyon, Arizona, showing final digital elevation model (DEM) from December 2004 with May 2002 orthophotography. DEM extent was clipped to remove vegetated areas, areas above the 2,746 cubic meters per second (m^3/s) flow line, and areas with no input data.

Table 5. Digital elevation model (DEM) summary statistics used in this study along the Colorado River corridor within Glen, Marble, and Grand Canyons, Arizona.

[m, meters; m^2, square meters; std. dev., standard deviation]

Survey date	Reach	Area (m^2)	Min (m)	Max (m)	Mean (m)	Std. dev. (m)
August 2000	2	293351	907.95	928.47	918.38	3.02
September 2000	2	347747	907.34	928.44	918.52	2.97
May 2002	2	345763	906.98	927.90	918.55	2.84
May 2004	2	319268	907.06	925.09	918.09	2.33
November 2004	2	338667	910.20	928.46	919.35	2.30
December 2004	2	347227	907.06	928.47	918.78	2.84
May 2002	3	245215	860.56	889.77	876.95	5.66
May 2004	3	170310	860.44	882.66	873.93	3.75
November 2004	3	254226	860.58	890.10	876.96	5.54
December 2004	3	255570	859.48	890.11	877.02	5.63
August 2000	4	292930	832.05	866.50	850.73	5.57
September 2000	4	299560	831.45	866.32	850.65	5.70
May 2002	4	308403	832.00	866.50	850.69	5.42
May 2004	4	276881	832.10	858.93	849.49	4.59
November 2004	4	317940	832.55	866.00	850.87	5.27
December 2004	4	313751	830.17	866.62	850.72	5.68
August 2000	5	445079	817.77	847.27	835.65	4.62
September 2000	5	457655	816.41	847.26	835.67	4.72
May 2002	5	532917	819.09	847.04	835.09	4.67
May 2004	5	440230	817.61	841.61	833.92	4.02
November 2004	5	544847	818.12	847.12	835.22	4.63
December 2004	5	535372	816.25	847.16	835.04	4.83
May 2002	6	349453	806.05	826.94	817.33	3.62
May 2004	6	289920	804.67	821.60	816.19	2.88
November 2004	6	332992	805.23	826.95	817.29	3.69
December 2004	6	328477	801.59	827.00	817.01	3.89
August 2000	7	373727	777.05	806.57	793.75	5.06
September 2000	7	422879	776.13	806.57	793.55	4.99
May 2002	7	548697	776.45	806.57	793.81	4.56
May 2004	7	483500	775.66	801.43	792.85	3.73
November 2004	7	391826	776.88	806.57	794.64	4.85
December 2004	7	428893	777.33	806.57	794.33	4.88

To make sure that the TIN model represented the ground, or bare-earth surface, it was necessary to remove spurious and (or) contradictory points from the input datasets and to prioritize the datasets to choose which dataset to use in areas of overlap (fig. 5). Lidar and photogrammetry points were processed to eliminate points associated with vegetated areas and standing water, as well as points that were lower than the 227-m^3/s stage elevation and higher than the 2,746-m^3/s stage elevation. All lidar and photogrammetry data collections were flown at a constant 227-m^3/s flow, so points lower than this elevation were removed using the 227-m^3/s stage elevation lines derived from the land-cover classifications.

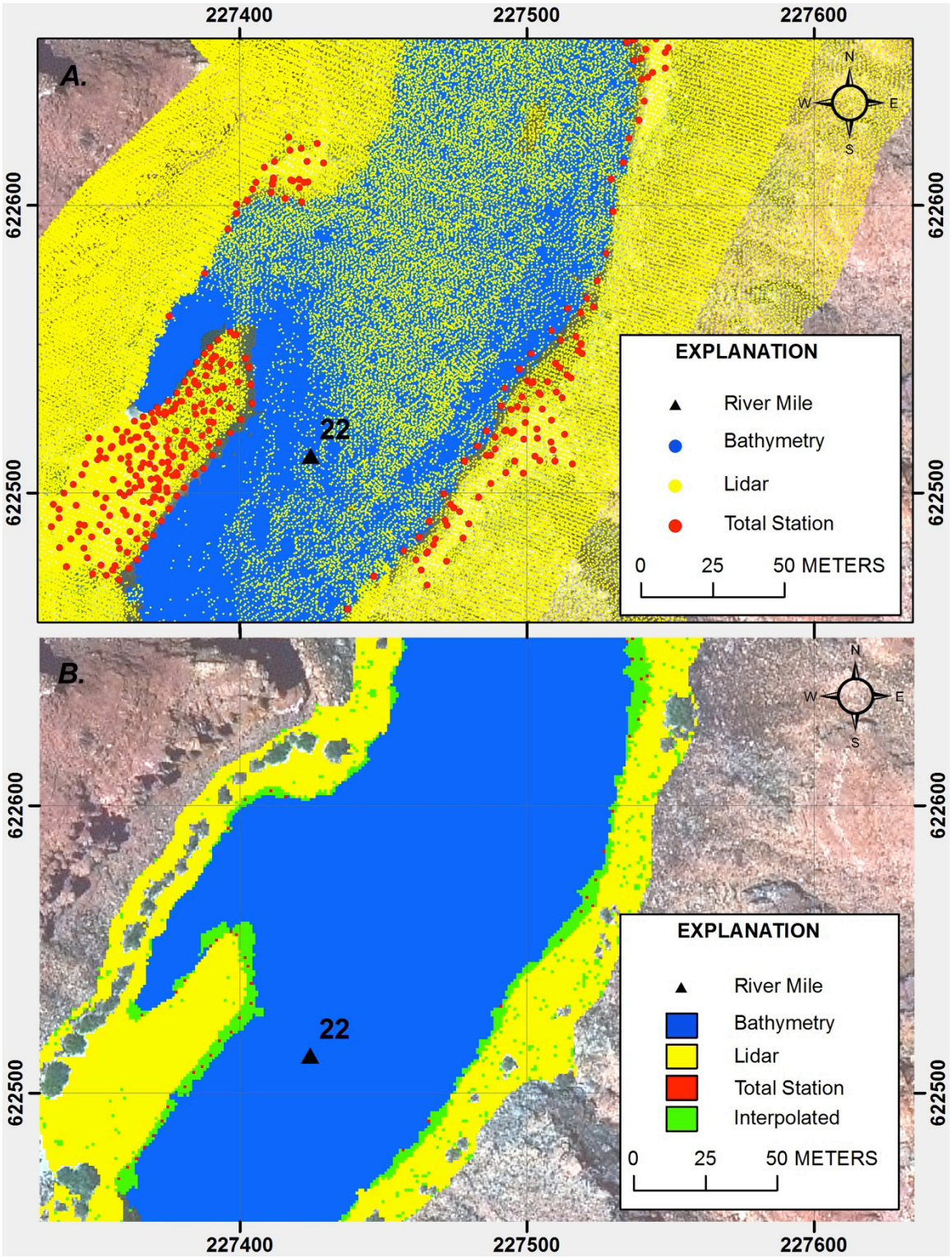

Figure 5. Maps of a part of reach 3 in Grand Canyon, Arizona, showing (*A*) the raw data points and (*B*) polygon boundaries used to exclude or prioritize the input datasets, clip triangulated irregular network (TIN) model and digital elevation models (DEMs), and generate uncertainty surfaces.

The largest post-dam flow release occurred in 1983 and was approximately 2,746 m^3/s . Therefore, we chose this level as the upper elevation limit to the lidar and photogrammetry datasets and points above this level were removed. The 2,746-m^3/s stage elevation was derived using a combination of (1) a one-dimensional flow model (Wiele and Griffin, 1997), (2) measured stage elevation at long-term sand-bar monitoring sites (Hazel and others, 2010), and (3) GIS surface extrapolation routines (Magirl and others, 2005). Lidar and photogrammetry points located adjacent to the 2,746-m^3/s stage elevation and having slopes greater than 45° (extreme slopes) were also removed. Bathymetric input files were processed to remove data points above 227 m^3/s to exclude any data collected at higher flows. For areas above the 227-m^3/s stage elevation, lidar and photogrammetry data were prioritized over TS points. For areas below the 227 m^3/s, bathymetric data were prioritized over TS points. TS points were only used in areas that occurred between the extent of the lidar and photogrammetry data and bathymetric data (fig. 5).

The absence of data for some parts of each study reach and the removal of bad data points discussed above resulted in gaps in the data coverage. Some of these gaps were left as voids and excluded from the final DEM, whereas some voids were interpolated across (fig. 5). We created several sets of polygons and associated rule sets to determine which areas to include in the DEM and which areas to exclude. The gaps typically occurred in areas where bathymetric measurements could not be made (such as rapids and riffles and shallow areas along the shoreline where depths were less than about 1.5 m), areas of dense vegetation and standing water, and areas where datasets do not overlap. In gaps within the lidar and photogrammetric data, the land-cover classification polygons were used to prevent TIN model generation within data voids.

Below the 227-m^3/s stage elevation, gaps typically occur in rapids and riffles and along the shoreline between the sonar data and the terrestrial data. Rapids and riffles were excluded from the DEM, whereas shoreline areas were typically interpolated across the DEM. Along steeply sloping shorelines, gaps between the bathymetric and terrestrial datasets were relatively narrow (approximately 2–4 m). However, along the shallow, low-angle sandbars, these distances were sometimes quite large (greater than 10 m). In many of these gaps around sandbars, TS points were collected below the water surface to depths of approximately 1–1.5 m and were used in TIN model construction. Gaps without TS point data were interpolated across only if the difference in elevation between the two datasets was less than 2 m. Following interpolation, TIN models were visually inspected for errors, which were manually corrected by editing the TIN. These errors typically involved erroneous lidar points near vegetation that were not clipped by the land-cover boundary and anomalous (erroneous) bathymetry points that were not deleted in the editing process.

An important aspect of DEM construction is selecting the proper grid resolution for the input datasets. The ideal grid resolution contains the same number of grid cells as data points (McCullagh, 1988). The grid-size estimator of Hu (2003) was used to determine if the combined datasets have the necessary point density to be reliably interpolated to a 1-m cell size. Hu (2003) proposed that DEM grid sizes can be estimated using the equation:

$$\text{DEM cell size} = \sqrt{\frac{Area}{Number\ of\ points}}.$$

This equation was applied to the edited and filtered hybrid point datasets for all 32 surveys. The results show a mean cell size of 0.97 m with a standard deviation of 0.16 m and indicate that a 1-m grid cell size is appropriate for our datasets.

A 1-m resolution DEM was derived for each survey (fig. 4; appendix 1). All DEMs for a particular reach were derived in the exact same orthogonal space. That is, they share the same cell resolution, cell centers, and bounding northing and easting coordinates. The end result is a set of coincident DEMs, which ensures that no resampling errors are introduced during change detection between surveys.

DEM Uncertainty

Accounting for uncertainty is a crucial component of monitoring studies that compare sequential DEMs to detect spatial patterns and volumes of morphological change (Brasington and others, 2003; Lane and others, 2003; Wheaton and others, 2010). In this context, our definition of uncertainty is limited to errors in the vertical component associated with comparison among the DEMs described in this study. Horizontal (positional) errors are considered negligible from the survey methods used here at the scale of 1-m resolution grid cells. Even in consideration of the vertical component of uncertainty, some components of error are not relevant. For example, because the same control points were used for each repeat survey, the uncertainty in the absolute position of the control points is not included in our uncertainty estimate. This places the focus solely on the uncertainty that is involved in creating a DEM independently for each of the survey methods used in the study. For each survey, the vertical component of uncertainty for each data type (lidar/photogrammetry, ground surveys, bathymetry) was estimated. This results in nine categories of spatially variable uncertainty estimates that depend on the specific survey method and date of survey. The uncertainty estimates were tabulated in raster format, coincident with the corresponding DEM that contains uncertainty values for each survey date. Interpolation uncertainty was not estimated for areas of no data input (interpolated areas), with the exception of areas covered by singlebeam bathymetric surveys.

Each interpolated area was assigned uncertainty according to the adjacent data collection method. Thus, for areas above the 227-m^3/s stage elevation, interpolated areas are assigned the appropriate lidar or photogrammetry uncertainty estimate. For areas below the 227-m^3/s stage elevation, interpolated areas are assigned the multibeam-sonar uncertainty estimate. The resulting uncertainty surfaces inherit spatial variability from the final survey method polygons (fig. 5) and have spatially uniform uncertainty estimates therein.

Several methods were used to estimate the vertical uncertainty associated with the datasets used to construct the DEMs, the details of which are discussed in later sections. Bathymetric uncertainty was estimated separately for multibeam and singlebeam datasets. Multibeam data were evaluated using a procedure that compares the elevations of the 1-m DEMs within areas of stable topography that have not changed over the course of this study. Such areas are referred to as fiducial surfaces, in the terminology of Brock and others (2001). For the singlebeam data, vertical uncertainty was estimated by combining a cross-line analysis of the precision within the surveys with the uncertainty associated with the interpolation of the singlebeam data to a 1-m DEM. The uncertainties associated with the lidar and photogrammetric datasets were estimated by comparing the elevations of points between individual surveys within fiducial areas that we are confident have not changed over the course of this study.

Four primary metrics are used to quantify uncertainty in the topographic and bathymetric datasets. These metrics are mean error in elevation (MEz), mean absolute error in elevation (MAEz), the root-mean-square error in elevation at the 68-percent confidence level (RMSEz), and root-mean-square error in elevation at the 95-percent confidence level (RMSEz 95%). These statistics are computed as follows:

$$\mathrm{MEz} = \sum_{i=0}^{n} \Delta EHi/\mathrm{n}, \quad (1)$$

$$\mathrm{MAEz} = \sum_{i=0}^{n} |\Delta EHi|/\mathrm{n}, \quad (2)$$

$$\mathrm{RMSEz} = \sqrt{\sum_{i=0}^{n} (\Delta EHi)^2/n}, \text{ and} \quad (3)$$

$$\mathrm{RMSEz\ 95\%} = 1.96 \times \mathrm{RMSEz}, \quad (4)$$

where ΔEH_i is the ellipsoid-height difference between corresponding points in two datasets. The standard deviation and skewness for each ellipsoid-height difference (ΔEH) distribution are also reported.

The primary intended use for the DEMs described in this study is to determine the net change in volume between different time periods. The MAEz metric represents the spatially distributed uncertainty for each DEM. The RMSEz and RMSEz 95-percent metrics are the elevation errors that are not expected to be exceeded at the 68- and 95-percent levels of confidence, respectively, and provide an estimate of the level of confidence in the elevation for each grid cell in the mapped area for each survey date. However, resolution of uncertainty at the level of each grid cell is more conservative than required when the primary interest is net change in storage over a large area. The RMSE metric uses the sum of squared difference values and, as a result, a relatively few large errors have a much greater influence on the RMSE value than do the dominant, smaller errors. The RMSE metric also varies in ways not related to the average error of a population (Willmott and Matsuura, 2005). The MEz represents the mean difference in elevation, or bias between surveys. However, because comparisons are pooled for different time periods for the multibeam data, if some surveys were high and other surveys low, the MEz may be near zero and not a measure of potential bias for any single survey (see section on Multibeam Uncertainty below). The MAEz metric provides a good estimate of the average uncertainty associated with repeat measurements that includes any potential bias, and it is this metric that best describes the uncertainties associated with the different data collection methods used to generate the DEMs presented in this report.

Bathymetry

Surface roughness or texture affects uncertainty in grid-cell elevations, regardless of survey method. For rough-textured surfaces, small errors in position can result in large errors in elevation, whereas for smoother surfaces, errors in position may result in very little error in elevation. Therefore, areas that have a high surface roughness, such as rocky shorelines, will inherently have higher uncertainties than areas that are relatively smooth, such as sand-bedded areas and shallow gravel bars (Wheaton and others, 2010). To more accurately represent the vertical uncertainty in the multibeam bathymetric topography, the surface roughness (or bed texture) within each surveyed surface was quantitatively classified into smooth and rough surface elements.

Bed-Texture Classification

Bed texture was classified into smooth and rough categories based on statistical analysis of the bathymetric data. High-resolution (0.25-m grid spacing) multibeam bathymetric data were used to generate hillshade raster images of the surfaces using an illumination angle of 90°, which is directly overhead (fig. 6*A*). A hillshade raster image scales the image intensity between 0 and 255 for each cell in the raster image. From the hillshade-image intensity values, the focal standard deviation (FSD) was calculated for each image cell using a 3×3-m moving window. The FSD grid values were then classified into rough (FSD less than 10) and smooth (FSD greater than or equal to 10) categories. The FSD separation value (10) was selected by trial and error and visual inspection. The selected FSD value resulted in a classification that best matched appearance in the hillshade images. The FSD separation value corresponds to adjacent-cell elevation differences of approximately 0.25 to 0.36 m. Within the smooth textural class, ellipsoid height differences ranged from 0.0 to 0.25 m, and within the rough textural class, ellipsoid height differences ranged from 0.36 to 0.9 m. The results from this hillshade-FSD classification were converted to polygons, restricting the minimum polygon area to be 25 m^2 (fig. 6*B*), which were, in turn, converted to 1-m grids that were coincident with the 1-m DEM (fig. 6*C*).

Multibeam Uncertainty

DEM uncertainty was estimated on smooth and rough channel beds by examining the ΔEH in the 1-m DEMs within fiducial areas (that is, areas that did not change appreciably in elevation within the 4-

year period of this study). The fiducial surfaces, which were at least 100 m^2 in area, were created as 1-m DEMs using the 1-m multibeam bathymetric data. Fiducial surfaces were identified in both smooth and rough bed-texture map classes. A total of 12 fiducial areas were selected in smooth areas, seven in rough areas, with at least one fiducial area defined in each reach (reaches 2 through 7 only). Figure 7 shows examples of rough and smooth fiducial polygons within reach 6.

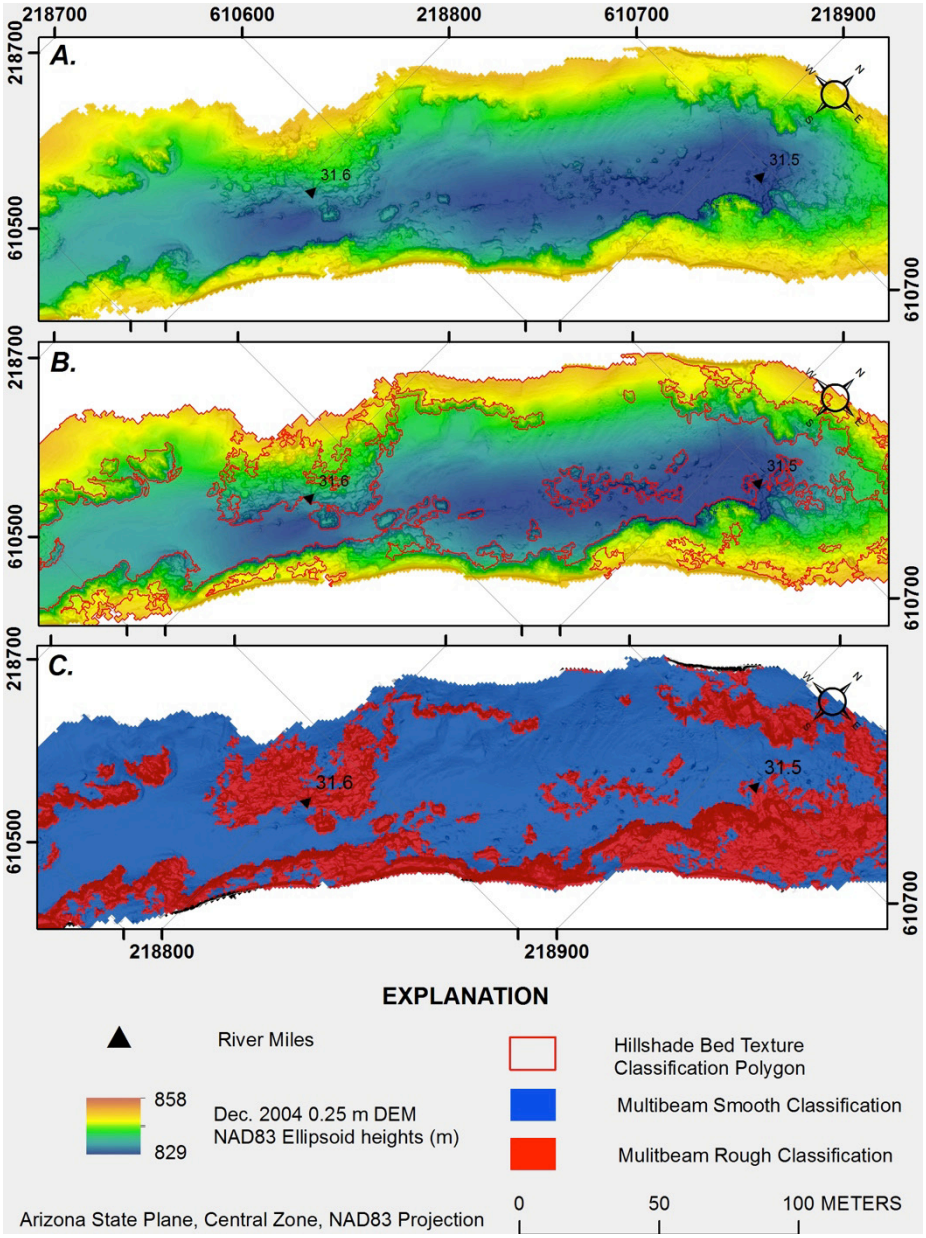

Figure 6. Maps of a part of reach 4 in Grand Canyon, Arizona, showing stages in the bed-texture classification process using the December 2004 survey data. *A*, 0.25-meter (m) digital elevation model (DEM) and hillshade derived from high-resolution mulitbeam bathymetric data. *B*, Bed-texture classification polygons superposed on the 0.25 m DEM and hillshade. For each cell in the hillshade grid, the focal standard deviation (FSD) was calculated using a 3×3-m picture-element array. Cells with FSD values greater than or equal to 10 were classified as rough, cells with FSD less than 10 were classified as smooth. Rough and smooth cells were aggregated into polygons with an area greater than 25 square meters (m^2) and converted into a 1-m grid. *C*, Final 1-m bed-texture classification grid superposed on the 0.25-m hillshade.

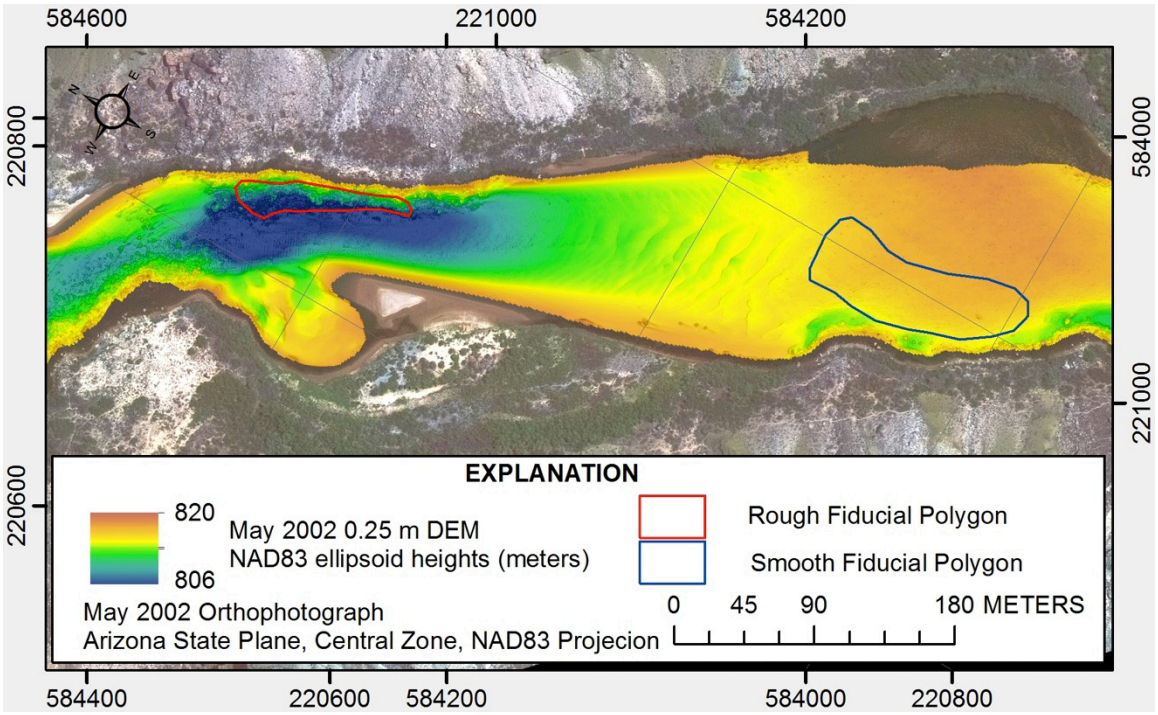

Figure 7. Map of a part of reach 6 in Grand Canyon, Arizona, showing examples of rough and smooth fiducial areas on a shaded-relief image derived from the May 2002 digital elevation model (DEM) superposed on the May 2002 orthophotography. Fiducial areas are assumed to not have changed in elevation over the course of the study and, as such, were used to generate uncertainty estimates for the multibeam data.

For smooth areas, the fiducial surfaces were defined on large gravel bars and relatively flat bedrock outcrops. For rough areas, fiducial surfaces were defined on steep talus slopes and boulder-dominated debris fans. For each survey date, every fiducial DEM grid cell was compared to its corresponding grid cells for all the other survey dates, which resulted in five temporal ΔEH comparisons for each grid cell. All grid cells from each fiducial area and temporal comparison were combined, or pooled, to derive one uncertainty estimate for each survey date (table 6). For example, the summary statistics for the August 2000 smooth bed classification were derived from a dataset that included ΔEH values from all 12 fiducial areas and all five temporal comparisons. The ΔEH populations all have skewness values that are less than 0.5, which indicates a fairly normal distribution. MAEz values average 0.07 m for smooth areas and 0.27 m for rough areas. Kaplinski and others (2009) used a cross-line analysis on the raw multibeam soundings to estimate uncertainty (precision) in the raw multibeam datasets; their results were similar to the results obtained for the DEM datasets, where the MAEz values ranged from 0.04 to 0.08 m. One advantage of using the fiducial-surface method is that the resulting uncertainties account for a number of sources of error involved in DEM production, which otherwise would need to be formulated and determined individually and summed. This technique provides a reasonable, standardized procedure for estimating uncertainty, where fiducial areas can be reliably established.

Table 6. Summary statistics of multibeam bathymetry uncertainty used in this study along the Colorado River corridor within Glen, Marble, and Grand Canyons, Arizona.

[MEz, mean error in elevation; MAEz, mean absolute error in elevation; RMSEz, root-mean-square error in elevation at the 68-percent confidence level; RMSEz 95%, root-mean-square error in elevation at the 95-percent confidence level; m, meters; n, number of observations]

Survey date	Bed class	n	MEz (m)	MAEz (m)	RMSEz (m)	RMSEz 95% (m)	Std. dev. (m)	Skewness
August 2000	smooth	95,905	-0.04	0.08	0.10	0.19	0.09	0.22
August 2000	rough	23,320	-0.02	0.34	0.45	0.89	0.45	0.05
September 2000	smooth	99,904	-0.01	0.08	0.10	0.20	0.10	0.07
September 2000	rough	30,098	0.00	0.33	0.44	0.86	0.44	0.07
May 2002	smooth	169,773	0.01	0.06	0.08	0.15	0.08	0.07
May 2002	rough	35,099	0.00	0.25	0.33	0.64	0.33	0.00
May 2004	smooth	169,958	0.00	0.07	0.09	0.17	0.09	-0.13
May 2004	rough	35,036	0.01	0.24	0.32	0.63	0.32	-0.03
November 2004	smooth	169,702	0.00	0.06	0.08	0.15	0.08	-0.10
November 2004	rough	35,062	0.01	0.22	0.29	0.57	0.29	-0.04
December 2004	smooth	163,647	0.01	0.06	0.08	0.15	0.08	0.04
December 2004	rough	44,053	0.02	0.23	0.32	0.62	0.31	-0.01

Singlebeam Uncertainty

Uncertainty analysis of singlebeam data requires a different approach because of interpolation uncertainty associated with generating a continuous surface from gridded transect lines. Uncertainty for the parts of the DEMs created from singlebeam surveys was estimated by partitioning the uncertainty into a component associated with survey precision and a component associated with DEM interpolation of the singlebeam data. Survey precision was estimated using cross-line checks (U.S. Army Corps of Engineers [USACE], 2002). A cross-line check compares the elevation (or depth) of intersection points from separate intersecting survey lines. Cross-line checks were conducted on eight individual singlebeam transects for each survey trip by selecting pairs of points that were within a 1-m radius. For each pair of points, the ΔEH was calculated. The ΔEH values from all cross-line checks were combined for each survey trip to derive an estimate of measurement uncertainty. The results of the cross-line analyses (table 7) show that both the August and September surveys were of good quality with a MEz less than 0.01 m (indicating minimal bias) and a RMSEz 95% less than 0.25 m, which exceed both USACE and International Hydrographic Organization standards for “special order” and surveys (USACE, 2002).

Table 7. Summary statistics of singlebeam bathymetry cross line check uncertainty used in this study along the Colorado River corridor within Glen, Marble, and Grand Canyons, Arizona.

[MEz, mean error in elevation; MAEz, mean absolute error in elevation; RMSEz, root-mean-square error in elevation at the 68-percent confidence level; RMSEz 95%, root-mean-square error in elevation at the 95-percent confidence level; m, meters; n, number of observations]

Survey date	n	MEz (m)	MAEz (m)	RMSE (m)	RMSE 95% (m)	Std. dev. (m)	Skewness
August 2000	545	0.00	0.07	0.10	0.19	0.10	0.33
September 2000	858	-0.01	0.07	0.10	0.19	0.10	0.10

The uncertainty associated with interpolating singlebeam-transect grids to a continuous surface was estimated by using a bootstrapping technique on surveys at one site (River Mile 32 in reach 4) with singlebeam surveys in both August and September 2000 (Efron and Tibshirani, 1998). The process involved partitioning the sorted singlebeam points into test and training subsets. The test subset consisted of a random sample of 10 percent of the original dataset that was withheld from the interpolation process (that is, DEM construction). DEMs were constructed with the remaining 90 percent of the original dataset and the resulting DEM cells were compared to the test subset to derive ΔEH values. The results of the comparison show MAEz interpolation errors of 0.13 and 0.07 m for the August and September surveys, respectively (table 8).

Table 8. Summary statistics of singlebeam interpolation uncertainty used in this study along the Colorado River corridor within Glen, Marble, and Grand Canyons, Arizona.

[MEz, mean error in elevation; MAEz, mean absolute error in elevation; RMSEz, root-mean-square error in elevation at the 68-percent confidence level; RMSEz 95%, root-mean-square error in elevation at the 95-percent confidence level; m, meters; n, number of observations]

Survey date	n	MEz (m)	MAEz (m)	RMSE (m)	RMSE 95% (m)	Std. dev. (m)	Skewness
August 2000	159	-0.01	0.13	0.24	0.47	0.24	-0.09
September 2000	210	0.01	0.07	0.09	0.17	0.09	-0.20

The total uncertainty applied to regions of the DEMs constructed from singlebeam surveys was obtained by computing the quadratic sum of the individual error components (Taylor, 1997) using the following equation:

$$\text{total uncertainty} = \sqrt{(\text{survey precision})^2 + (\text{interpolation uncertainty})^2}.$$

Using the MAEz statistic from tables 7 and 8, the total uncertainty for singlebeam data is 0.15 m for the August 2000 surveys and 0.10 m for the September 2000 surveys.

Lidar and Photogrammetry Uncertainty

Estimates of lidar and photogrammetric vertical uncertainties were derived from the ΔEH between the different temporal airborne data collections for fiducial areas within reach 5 (table 9). Fiducial points were selected using the following criteria: (1) the bare, smooth land-cover units above the 1,274-m^3/s stage elevation, (2) slopes of less than 12 degrees, (3) points more than 1 m from dense or sparse vegetation landform classifications, and (4) points not in the vicinity of abrupt changes in slope (Maune and others, 2007). In addition, the points were visually inspected with imagery to exclude areas that appeared to have changed. The results of the comparison show that MAEz values range from 0.17 to 0.21 m.

Table 9. Summary statistics of lidar and Photogrammetry uncertainty used in this study along the Colorado River corridor within Glen, Marble, and Grand Canyons, Arizona.

[MEz, mean error in elevation; MAEz, mean absolute error in elevation; RMSEz, root-mean-square error in elevation at the 68-percent confidence level; RMSEz 95%, root-mean-square error in elevation at the 95-percent confidence level; m, meters; n, number of observations]

Survey date	n	MEz (m)	MAEz (m)	RMSEz (m)	RMSEz 95% (m)	Std. dev. (m)	Skewness
August 2000	754590	-0.02	0.18	0.26	0.51	0.26	-0.71
September 2000	755694	-0.02	0.18	0.26	0.50	0.26	-0.72
May 2002	824240	-0.02	0.21	0.28	0.56	0.28	-0.49
November 2004	829324	0.00	0.17	0.23	0.45	0.23	-0.44
December 2004	825070	-0.05	0.17	0.23	0.46	0.23	-0.39

Uncertainty Surfaces

For each DEM, a map was created that depicts uncertainty for each cell within each DEM. Assignment of each cell's uncertainty was based on the type of data that was used to determine the elevation for that cell in the final DEM (fig. 8*A*). Owing to the multiple sources of data used to generate the final DEM, this required generating a grid that identified the data source or method of interpolation for each cell (fig. 8*B*). Inclusion of all data sources and interpolation methods results in nine data-source categories—(1) lidar, (2) photogrammetry, (3) multibeam over rough bed, (4) multibeam over smooth bed, (5) singlebeam, (6) TS points above the 227-m^3/s stage elevation, (7) TS points below the 227-m^3/s stage elevation, (8) interpolated areas above the 227-m^3/s stage elevation, and (9) interpolated areas below the 227-m^3/s stage elevation. MAEz values were assigned to each cell based on the data source category (fig. 8*C*); table 10). Lidar and (or) photogrammetry uncertainty values were assigned to TS points and interpolated areas above the 227-m^3/s stage elevation (classes 6 and 8), and multibeam smooth bed uncertainties were assigned to TS points and interpolated areas below the 227-m^3/s stage elevation (classes 7 and 9). Interpolated areas constitute less than 10 percent of the total DEM area, and the majority of these areas are sufficiently well constrained by flanking data points that it was deemed appropriate to apply the calculated uncertainty of the surrounding data points. For example, the majority of interpolated areas occur below the 227-m^3/s stage elevation in shallow sandbar and gravel-bar areas with low surface roughness and slope (fig. 8*A*). Within these areas, the TIN model creates surface area between data points (either total station or multibeam) that sufficiently captures the topography surrounding the data point. A small part of the interpolated areas undoubtedly incur uncertainty beyond that of the surrounding data points. Future studies should consider investigating methods for applying an additional interpolation term to the uncertainty in these areas.

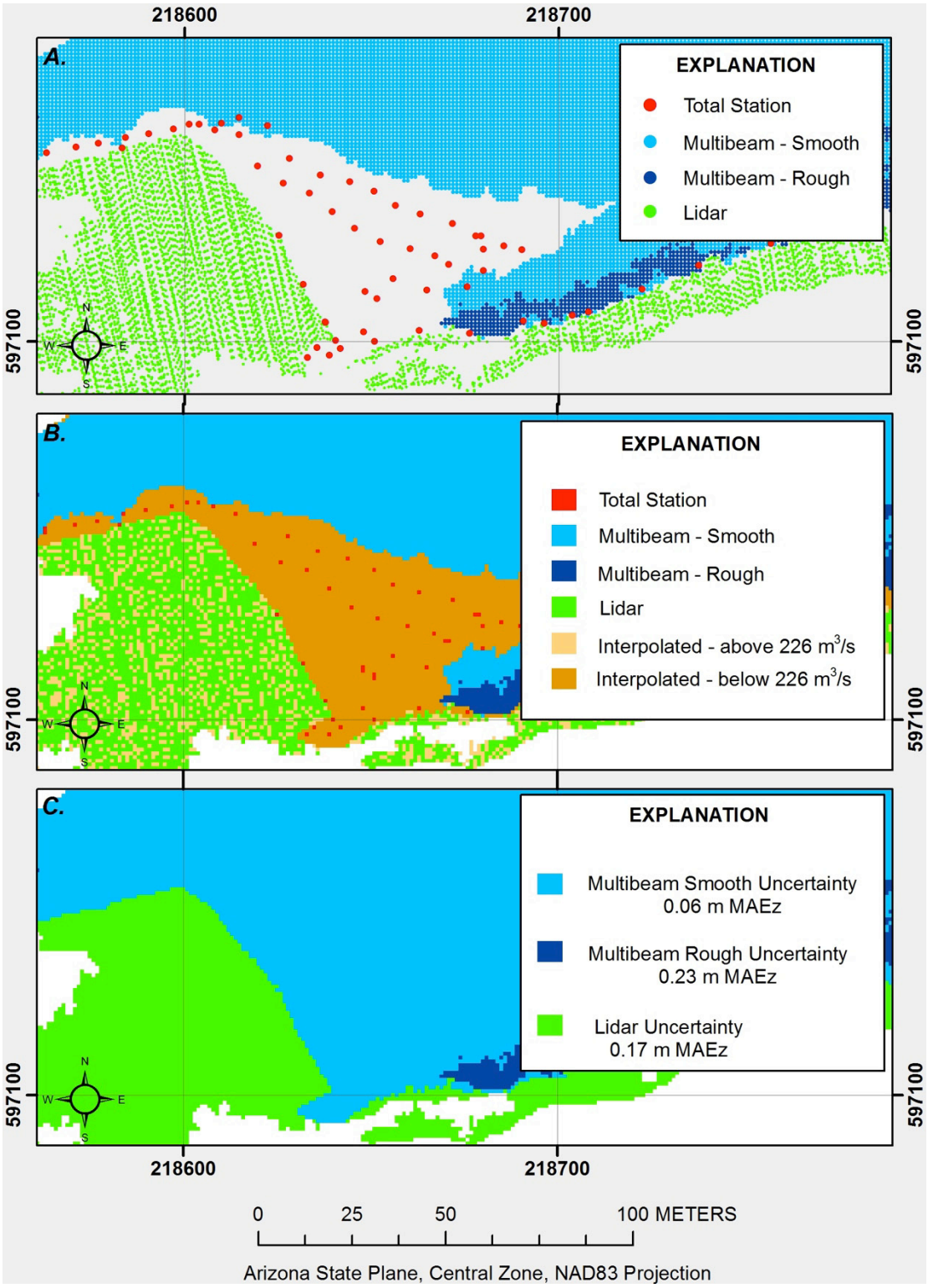

Figure 8. Maps of a part of reach 5 in Grand Canyon, Arizona, showing the stages involved in assigning uncertainty values using the November 2004 survey data—*A*, data points; *B*, raster image of input data sources; and *C*, uncertainty surface generated for the November 2004 digital elevation model (DEM). M, meters; m^3/s, cubic meters per second; MAEz, mean absolute error in elevation.

Table 10. Uncertainty estimates assigned to each data source category in final digital elevation models (DEMs) for the Colorado River corridor within Glen, Marble, and Grand Canyons, Arizona.

[m^3/s, cubic meters per second; n.a., not applicable]

Data source category[1]	August 2000	September 2000	May 2002	May 2004	November 2004	December 2004
Lidar	0.18	0.18	n.a.	n.a.	0.17	0.17
Photogrammetry	n.a.	n.a.	0.21	n.a.	n.a.	n.a.
Multibeam—smooth	0.08	0.08	0.06	0.07	0.06	0.06
Multibeam—rough	0.34	0.33	0.25	0.24	0.22	0.23
Singlebeam	0.15	0.10	n.a.	n.a.	n.a.	n.a.
Total station above 227 m^3/s	0.18	0.18	0.21	0.10	0.17	0.17
Total station below 227 m^3/s	0.08	0.08	0.06	0.07	0.06	0.06
Interpolated above 227 m^3/s	0.18	0.18	0.21	0.10	0.17	0.17
Interpolated below 227 m^3/s	0.08	0.08	0.06	0.07	0.06	0.06

[1]MAEz (root-mean-square error in elevation at the 68-percent confidence level) statistics from tables 5 through 8 were used for each data source category.

Summary

One meter DEMs were constructed for six study reaches along the Colorado River in Grand Canyon. The DEMs combine elevations determined from ground-based total station surveys, airborne remote-sensing missions, and sonar bathymetric surveys collected in in August 2000, September 2000, May–June 2002, May–June 2004, November 2004, and December 2004.

The general approach to DEM construction was to create a TIN model from the input datasets, then interpolate a 1-m raster DEM from the TIN model. Lidar and photogrammetry points were processed to eliminate anomalous spikes, vertical offsets, planimetric shifts, regional tilts, and to exclude points on or near vegetated areas, standing water, and for points higher than the 2,746-m^3/s stage elevation. Bathymetry surveys excluded rapids and riffles and shallow areas along the shoreline, where depths were less than about 1.5 m. In areas along the shoreline lacking bathymetric point data, TS points collected by total station were used constrain the TIN model. Clipping polygons were generated that outlined the perimeter of the combined datasets and internal spatial gaps in the point datasets. The TIN models were formed and then clipped with the internal and external (perimeter) clipping polygons.

The final TIN model was used to create a 1-m resolution DEM for each survey. All DEMs were derived to be coincident with each other. That is, they share the same cell resolution, and cell centers, and bounding northing and easting coordinates. The end result is a set of coincident DEMs. This step ensures that no resampling errors are introduced during change detection between surveys.

Statistics were used to construct uncertainty grids that are coincident with the DEMs. For each survey period, the vertical component of uncertainty was estimated for each data type and for two different areas of bed-surface texture. These estimates of uncertainty were applied regionally to the uncertainty grid, depending on which data type was used in DEM construction. Even though the uncertainty estimates were spatially uniform by method, because the DEMs were produced by hybrid data sources the resulting uncertainty estimates varied spatially. Interpolated areas, or areas not constrained by data points, constituted less than 10 percent of the DEM area and were assigned uncertainty estimates from surrounding areas where the uncertainty was defined. Vertical uncertainty estimates range from 0.17 to 0.21 m within the lidar and photogrammetry parts of the DEMs, from 0.06 to 0.08 m within areas classified as multibeam smooth, and between 0.22 to 0.34 m within areas classified as mulitbeam rough (table 10). Therefore, the range of vertical change that can be reasonably detected (that is, change above the quadratic sum of the uncertainty estimates from the surfaces being compared) varies from 0.08 to 0.01 m for regions within the multibeam smooth classification, 0.24 to 0.28 m from regions within the lidar and photogrammetry classification, and 0.32 to 0.47 m for regions within the multibeam rough classification.

The resulting DEMs from this study will provide valuable information to the ongoing efforts to assess the effects of GCD operations on the CRE. The DEMs can be used by researchers to map the spatial characteristics of the geomorphic change within the study reaches and to estimate sediment budgets for different time periods by calculating the difference in volume between surveys. In addition, the DEMs provide valuable boundary conditions for numerical models of sediment transport and deposition, as well as help define the spatial distribution of habitat for fisheries investigations.

Acknowledgments

This study was funded by the Bureau of Reclamation as part of the Glen Canyon Dam Adaptive Management Program. The authors wish to thank the multitudes of people involved in the data collection and processing.

References Cited

Bowen, Z.H., and Waltermire, R.G., 2002, Evaluation of light detection and ranging (LIDAR) for measuring river corridor topography: Journal of American Water Resources Association, v. 38, 33–41.

Brasington, J., Langham, J., Rumsby, B., 2003, Methodological sensitivity of morphometric estimates of coarse fluvial sediment transport: Geomorphology, v. 53, p. 299–316.

Brock, J.C., Sallenger, A.H., Krabill, W.B., Swift, R.N., and Wright, C.W., 2001, Recognition of fiducial surfaces in LiDAR surveys of coastal topography: Photogrammetric Engineering and Remote Sensing, v. 67, p. 1245–1258.

Crombaghs, M., Brügelmann, R., and deMin, E., 2000, On the adjustment of overlapping strips of laser altimeter height data: International Archives of Photogrammetry and Remote Sensing, v. 33, no. 3A, p. 230–237.

Crombaghs, M., Elberink, S.O., Brügelmann, R., and deMin, E, 2002, Assessing height precision of laser altimetry DEMs: International Society for Photogrammetry and Remote Sensing Technical Commission III Symposium 2002, "Photogrammetric Computer Vision," PVC02, September 9–13, 2002, Graz, Austria, A85–A90.

Davis, P., 2004, Review of results and recommendations from the GCMRC 2000–2003 remote-sensing initiative for monitoring environmental resources within the Colorado River ecosystem: U.S. Geological Survey Open-File Report 2004-1206, 73 p., available at http://pubs.usgs.gov/of/2004/1206/.

Doyle, D.R., 1994, Development of the National Spatial Reference System: Silver Spring, Maryland, National Geodetic Survey, accessed February 20, 2014, at http://www.ngs.noaa.gov/PUBS_LIB/develop_NSRS.html.

Efron, B., and Tibshirani, R.J., 1998, An introduction to the bootstrap: London , Chapman & Hall/CRC, 436 p.

Filin, S., 2003, Recovery of systematic biases in laser altimetry data using natural surfaces: Photogrammetric Engineering and Remote Sensing, v. 69, p. 1235–1242.

Gloss, S.P., Lovich, J.E., and Melis, T.S., eds., 2005, The state of the Colorado River ecosystem in Grand Canyon: U.S. Geological Survey Circular 1282, 220 p. (Also available at http://pubs.usgs.gov/circ/1282/.)

Grams, P.E., Topping, D.J., Schmidt, J.C., Hazel, J.E., and Kaplinski, M., 2013, Linking morphodynamic response with sediment mass balance on the Colorado River in Marble Canyon—Issues of scale, geomorphic setting, and sampling design: Journal of Geophysical Research, v. 118, 21 p, doi:10.1002/jgrf.20050.

Hazel, J., Jr., Topping, D.J., Schmidt, J.C., and Kaplinski, M., 2006, Influence of a dam on fine sediment storage in a canyon river: Journal of Geophysical Research, v. 111, 16 p.

Hazel, J.E., Jr., Kaplinski, M., Parnell, R.A., Kohl, K., and Schmidt, J.C., 2008, Monitoring fine-grained sediment in the Colorado River Ecosystem, Arizona-Control network and conventional survey techniques: U.S. Geological Survey Open-File Report 2008–1276, 15 p., available at http://pubs.usgs.gov/of/2008/1276/.

Hazel, J.E., Jr., Grams, P.E., Schmidt, J.C., and Kaplinski, M., 2010, Sandbar response following the 2008 high-flow experiment on the Colorado River in Marble and Grand Canyons: U.S. Geological Survey Scientific Investigations Report 2010–5015, 52 p., available at http://pubs.usgs.gov/sir/2010/5015/.

Hodgson, M.E., Jensen, J.R., Schmidt, S., Schill, S., and Davis, B., 2003, An evaluation of LIDAR- and IFSAR-derived digital elevation models in leaf-on conditions with USGS Level 1 and Level 2 DEMs: Remote Sensing of Environment, v. 84, p. 295–308.

Hu, Y., 2003, Automated extraction of digital terrain models, roads and buildings using airborne LiDAR data: University of Calgary, Department of Geomatics Engineering, UCGE report 20187, Ph.D. dissertation, 206 p.

Kager, H., and Kraus, K., 2001, Height discrepancies between overlapping laserscanner strips: Proceedings of Optical 3D Measurement Techniques V, October 1–4, Vienna, Austria, p. 103–110.

Kaplinski, M., Hazel, J.E., Parnell, R., Breedlove, M., Kohl, K., and Gonzales, M., 2009, Monitoring Fine-Sediment Volume in the Colorado River Ecosystem, Arizona: Bathymetric Survey Techniques, U.S. Geological Survey Open-File Report 2009-1207, 41 p., available at http://pubs.usgs.gov/of/2009/1207/.

Lane, S.N., Westaway, R.M., Hicks, D.M., 2003, Estimation of erosion and deposition volumes in a large, gravel-bed, braided river using synoptic remote sensing: Earth Surface Processes and Landforms, v. 28, p. 249–271.

Logan, B., Nelson, J., McDonald, R., and Wright, S., 2010, Mechanics and modeling of flow, sediment transport and morphological change in riverine lateral separation zones, *in* Hydrology and sedimentation for a changing future—Existing and emerging issues: Joint Federal Interagency Conference 2010, Federal Ineragency Hydrologic Modeling, 4th, and Federal Interagency Sedimentation, 9th, Las Vegas, Nev., June 27–July 1, Proceedings, CD-ROM, ISBN: 978-0-9779007-3-2.

Maas, H.-G., 2000, Least-squares matching with airborne laserscanning data in a TIN structure: International Archives of Photogrammetry and Remote Sensing, v. 33, part B3/1, p. 548–555.

Maas, H.-G., 2002, Methods for measuring height and planimetry discrepancies in airborne laserscanner data: Photogrammetric Engineering and Remote Sensing, v. 68, p. 933–940.

Magirl, C.S., Webb, R.H., and Griffiths, P.G., 2005, Changes in the water surface profile of the Colorado River in Grand Canyon, Arizona, between 1923 and 2000: Water Resources Research, v. 41, no. 5, W05021, doi:10.1029/2003WR002519.

Maune, D., Maitra, J., and McKay, E., 2007, Accuracy standards, *in* Maune, D.F., ed., Digital elevation model technologies and applications—The DEM users manual, 2nd edition: Bethesda, Md., American Society for Photogrammetry and Remote Sensing, chap. 3, p. 65–94,

McCullagh, M.J., 1988, Terrain and surface modeling systems—Theory and practice: Photogrammetric Record, v. 12, no. 72, p. 747–779.

Peng, M.-H., and Shih, T.-Y., 2006, Error assessment in two lidar-derived TIN datasets: Photogrammetric Engineering and Remote Sensing, v. 72, p. 933–947.

Postolov, V., Krupnik, A., and McIntosh, K., 1999, Registration of airborne laser data to surface generated by photogrammetric means: International Archives of Photogrammetry and Remote Sensing, v. 32, 3-W14, p. 95–100.

Raber, G.T., Jensen, J.R., Schill, S.R., and Schuckman, K., 2002, Creation of digital terrain models using an adaptive lidar vegetation point removal process: Photogrammetric Engineering and Remote Sensing, v. 68, p. 1307–1315.

Saleh, R.A., Chayes, D.N., Dasler, J.L., Doyle, D.R., Sanchez, R., Renslow, M.S., and Rose, J.J., 2003, Survey protocol evaluation program: Final report submitted to the Grand Canyon Monitoring and Research Program, accessed August 17, 2008, at http://www.gcmrc.gov/library/reports/GIS/Saleh2003.pdf.

Schmidt, J.C., and Graf, J.B., 1990, Aggradation and degradation of alluvial sand deposits, 1965 to 1986, Colorado River, Grand Canyon National Park, Arizona: U.S. Geological Survey Professional Paper 1493, 74 p.

Schmidt, J.C., Topping, D.J., Rubin, D.M., Hazel, J.E., Jr., Kaplinski, M., Wiele, S.M., and Goeking, S.A., 2007, Streamflow and sediment data collected to determine the effects of low summer steady flows and habitat maintenance flows in 2000 on the Colorado River between Lees Ferry and Bright Angel Creek, Arizona: U.S. Geological Survey Open-File Report 2007–1268, 79 p., available at http://pubs.usgs.gov/of/2007/1268/.

Taylor J.R., 1997, An Introduction to error analysis—The study of uncertainties in physical measurements, second edition: Sausalito, Calif., University Science Books.

Topping, D.J., Rubin, D.M., Nelson, J.M., Kinzel, P.J., III, and Corson, I.C., 2000, Colorado River Sediment Transport; part 1—Natural sediment supply limitation and the influence of Glen Canyon Dam: Water Resources Research, v. 36, p. 515–542.

Topping, D.J., Rubin, D.M., Grams, P.E., Griffiths, R.E., Sabol, T.A., Voichick, N., Tusso, R.B., Vanaman, K.M., and McDonald, R.R., 2010, Sediment transport during three controlled-flood experiments on the Colorado River downstream from Glen Canyon Dam, with implications for eddy-sandbar deposition in Grand Canyon National Park: U.S. Geological Survey Open-File Report 2010-1128, 111 p., available at http://pubs.usgs.gov/of/2010/1128/.

U.S. Army Corps of Engineers [USACE], 2002, Hydrographic surveying, draft engineer manual EM 1110-2-1003: Washington, D.C., U.S Army Corps of Engineers, 506 p., accessed September 24, 2009, at http://140.194.76.129/publications/eng-manuals/em1110-2-1003/toc.htm.

U.S. Geological Survey, 2006, Colorado mileage system [spatial database, GIS.BASE_GCMRC_TenthMile], 1st revised ed.: U.S. Geological Survey Grand Canyon Monitoring and Research Center Web site, accessed February 20, 2014, at http://www.gcmrc.gov/gis/silvermap1.aspx.

U.S. Department of the Interior, 1995, Operations of Glen Canyon Dam final environmental impact statement: Salt Lake City, Utah, Bureau of Reclamation, Upper Colorado Region, 337 p., accessed February 20, 2014, at http://www.usbr.gov/uc/envdocs/eis/gc/gcdOpsFEIS.html

Webb, R.H., Wegner, D.L., Andrews, E.D., Valdez, R.A., and Patten, D.T., 1999, Downstream effects of Glen Canyon Dam on the Colorado River in Grand Canyon—A review, *in* The controlled flood in Grand Canyon, Webb, R.H., Schmidt, J.C., Marzolf, G.R., and Valdez, R.A., eds.: Washington, D.C., American Geophysical Union, Geophysical Monograph 110, p. 1–21.

Wheaton, J.M., Brasington, J., Darby, S.E., and Sear, D.A., 2010, Accounting for uncertainty in DEMs from repeat topographic surveys—Improved sediment budgets: Earth Surface Processes and Landforms, v. 35, p. 136–156, doi:10.1002/esp.1886.

Wiele, S.M., and Griffin, E.R., 1997, Modification to a one-dimensional model of unsteady flow in the Colorado River through the Grand Canyon, Arizona: U.S. Geological Survey Water-Resources Investigations Report 97–4046, 17 p.

Willmott, C.J., and Matsuura, K., 2005, Advantages of the mean absolute error MAE over the root mean square error RMSE in assessing average model performance: Climate Research, v. 30, p. 79–82.

Wright, S.A., Melis, T.S., Topping, D.J., and Rubin, D.M., 2005, Influence of Glen Canyon Dam operations on downstream sand resources of the Colorado River in Grand Canyon, *in* Gloss, S.P., Lovich, J.E., and Melis, T.S., eds., The state of the Colorado River ecosystem in Grand Canyon: U.S. Geological Survey Circular 1282, p. 17–31.

Zilkoski, D.B., D'Onofrio, J.D. and Frakes, S.J., 1997, Guidelines for Establishing GPS-Derived Ellipsoid Heights, Standards—2 cm and 5 cm, Version 4.3: Silver Springs, Md., National Oceanic and Atmospheric Administration, National Geodetic Survey, Technical Memorandum NOS NGS-58, 22 p.